

1 ~~Intensified~~Sustained intensification of the Aleutian Low induces  
2 weak ~~tropical~~ Pacific ~~Decadal Variability~~ sea surface warming

3  
4 William J. Dow<sup>1</sup>, Christine M. McKenna<sup>1</sup>, Manoj M. Joshi<sup>2</sup>, Adam T. Blaker<sup>3</sup>, Richard Rigby<sup>1</sup>,  
5 Amanda C. Maycock<sup>1</sup>

6  
7 <sup>1</sup>School of Earth and Environment, University of Leeds, Leeds, UK

8 <sup>2</sup>Climatic Research Unit, School of Environmental Sciences, University of East Anglia, Norwich,  
9 UK

10 <sup>3</sup>National Oceanography Centre, Southampton, UK  
11  
12  
13  
14  
15  
16

17 **Abstract**

18  
19 **The**  
20 ~~It has been proposed that externally forced trends in the Aleutian Low drives decadal variability in~~  
21 ~~North Pacific sea surface temperatures (SST), but its role in basin-wide can induce a basin-wide~~  
22 ~~Pacific SST variability is less clear owing to the difficulty of disentangling coupled atmosphere-~~  
23 ~~ocean processes. We~~response that projects onto the pattern of the Pacific Decadal Oscillation  
24 ~~(PDO). To investigate this hypothesis, we~~ apply local atmospheric nudging ~~in an intermediate~~  
25 ~~complexity climate model~~ to isolate the effects of an ~~intense~~~~intensified~~ winter Aleutian Low ~~using~~  
26 ~~an intermediate complexity climate model sustained over several decades.~~ An ~~intensified~~  
27 ~~intensification of the~~ Aleutian Low produces a basin-wide SST response with a similar pattern to  
28 ~~the model's~~ internally-generated ~~Pacific Decadal Oscillation (PDO)-PDO.~~ The amplitude of the  
29 SST response in the North Pacific is comparable to ~~the~~ PDO, but in the tropics and southern  
30 subtropics the anomalies induced by the ~~intense~~~~imposed~~ Aleutian Low ~~anomaly~~ are a factor of 3  
31 weaker ~~than for the internally-generated PDO.~~ The tropical Pacific warming peaks in boreal spring,  
32 though anomalies persist year-round. A heat budget analysis shows the northern subtropical  
33 Pacific SST response is predominantly driven by anomalous surface ~~turbulent~~ heat fluxes in boreal

Formatted: Header

Style Definition: Normal: Font color: Auto, English (United Kingdom), Ligatures: None, Left, Indent: Left: 0 cm, First line: 0 cm, Space After: 0 pt, Line spacing: Multiple 1.15 li

Style Definition: Heading 1: Font: 20 pt, Not Bold, Font color: Auto, Ligatures: None, Space Before: 20 pt, After: 6 pt, Line spacing: Multiple 1.15 li, No bullets or numbering

Style Definition: Heading 2: Font: 16 pt, Not Bold, Font color: Auto, Ligatures: None, Space Before: 18 pt, After: 6 pt, Line spacing: Multiple 1.15 li, No bullets or numbering

Style Definition: Line Number: Font: (Default) Times New Roman, 10 pt, Font color: Auto

Formatted: Space After: 0 pt, Line spacing: 1.5 lines

Formatted: Font: 16 pt, Not Bold

Formatted: Font: 16 pt, Not Bold

Formatted: Font: 18 pt

Formatted: Indent: Left: 0 cm, Right: 0 cm, Space After: 0 pt, Line spacing: 1.5 lines

Formatted: Font color: Blue

Formatted: Space After: 0 pt, Line spacing: 1.5 lines

Formatted: Indent: Left: 0 cm, Right: 0 cm, Space After: 0 pt, Line spacing: 1.5 lines

Formatted: Font: 11 pt, Bold

Formatted: Font: Bold

Formatted: Normal, Indent: Left: 0 cm, Line spacing: 1.5 lines

Formatted: Justified, Right: 0 cm, Space After: 0 pt, Pattern: Clear (Background 1)

Formatted: Font color: Auto

34 winter, while in the equatorial Pacific the response is mainly due to meridional heat advection in  
35 boreal spring. The propagation of anomalies from the extratropics to the tropics can be explained  
36 by the seasonal footprinting mechanism, involving the wind-evaporation-SST feedback. The  
37 results show that low frequency variability and trends in the Aleutian Low could contribute to basin-  
38 wide anomalous Pacific SST, but the magnitude of the effect ~~cannot explain~~ the ~~full amplitude~~  
39 ~~of tropical Pacific, even for~~ the ~~PDO. This finding suggests that extreme Aleutian Low forcing~~  
40 ~~applied here, is small. Therefore,~~ external forcing of the Aleutian Low is unlikely to ~~explain~~ ~~account~~  
41 ~~for~~ observed ~~shifts~~ ~~decadal SST trends~~ in the ~~phase of PDO~~ ~~tropical Pacific~~ in the late 20th and  
42 early-21st centuries. ▲

Formatted: Header

Formatted: Font color: Custom Color( RGB(32,31,30) )

47 Key points (140 chars)

Formatted: Justified, Indent: Left: 0 cm, Right: 0 cm,  
Space After: 0 pt, Line spacing: 1.5 lines

49 ~~Relaxing towards a strong~~

- 50 1. ~~A sustained intensification of the~~ winter Aleutian Low produces ~~weak~~ warming ~~across~~ ~~in~~ the  
51 ~~equatorial~~ ~~tropical~~ Pacific that peaks in ~~boreal~~ spring.
- 52 2. Changes to surface heat fluxes (subtropics) during boreal winter and meridional advection  
53 (equatorial) during boreal spring in the upper ocean drive the SST warming.
- 54 3. A combination of the seasonal footprint mechanism and wind-evaporation-SST mechanism  
55 generate the surface climate anomalies in the tropical Pacific.

Formatted: Justified, Right: 0 cm, Line spacing: 1.5  
lines, Outline numbered + Level: 1 + Numbering Style:  
1, 2, 3, ... + Start at: 1 + Alignment: Left + Aligned at:  
0.63 cm + Indent at: 1.27 cm

|

| 60  
| 61  
| 62  
| 63

Formatted: Header

64 **1. Introduction**

65 \_\_\_\_\_

66 \_\_\_\_\_

67 The Aleutian Low has a well-known role in determining the North Pacific component of the Pacific-

68 Decadal Oscillation (PDO) (e.g. Schneider and Cornuelle, 2005; Zhang et al., 2018; Hu and Guan,

69 2018; Sun and Wang, 2006; Newman et al. 2016). Fluctuations in ~~the~~ Aleutian Low intensity affect

70 the North Pacific subpolar gyre (Pickart et al. 2008), upper ocean temperatures (e.g. Latif and

71 Barnett, 1996) and sea surface height (Nagano and Wakita, 2019) through anomalous thermal

72 forcing and wind stress. Oceanic Rossby waves initiated by Aleutian Low variability can propagate

73 westward and cause lagged signals in the Kuroshio-Oshashio Extension (KOE) region (e.g., Kwon

74 and Deser, 2007).

Formatted: Header

Formatted: Font: 11 pt, Bold

Formatted: Font: Bold

Formatted: Normal, Justified, Indent: Left: 0 cm, First line: 0 cm, Line spacing: 1.5 lines

Formatted: Justified, Indent: Left: 0 cm, Right: 0 cm, Line spacing: 1.5 lines

75

76 The ~~prevailing traditional~~ paradigm for the PDO ~~regards describes~~ the ~~role integrated effect~~ of the

77 ~~Aleutian Low to be largely driven by mid-latitude stochastic variability, which induces SST~~

78 ~~anomalies through turbulent heat flux and wind stress curl anomalies, and driving from~~ tropical

79 processes (~~ENSO variability~~) via excitation of ~~upper tropospheric~~-Rossby ~~waves wave trains and~~

80 ~~tropical-extratropical teleconnections~~ (Newman et al. 2016; Zhao et al. 2021; Vimont. 2005;

81 Knutson and Manabe 1998; Jin 2001). ~~We note that recent definitions separate low frequency~~

82 ~~PDO variability and show this is predominantly associated with stochastic extratropical~~

83 ~~atmospheric variability (i.e. the Aleutian Low) (Wills et al., 2018, 2019)~~. However, decadal changes

84 in the Aleutian Low may arise via other mechanisms including Arctic sea ice trends (Simon et al.

85 2021; Deser et al. 2016), ~~Arctic~~-stratospheric ~~polar vortex~~ variability (Richter et al., 2015), or as a

86 local response to external forcings (Smith et al. 2016; Dow et al. 2021; Dittus et al. 2021; Klavans

87 et al. submitted). It has been proposed that observed shifts in the PDO in the late 20th and early

88 21st centuries were driven by anthropogenic forcing of the Aleutian Low, which was then

89 communicated to a basin-wide PDO signal (Smith et al. 2016; Klavans et al. submitted; ~~Gan et al.~~

90 ~~2017~~). However, the mechanisms via which North Pacific anomalies linked to decadal Aleutian

91 Low changes may be communicated into a basin-wide SST response ~~including the tropics~~, and

92 whether the amplitude of such a response matches observed variations, remain unclear.

Formatted: Justified, Space After: 0 pt, Line spacing: 1.5 lines

Formatted: Justified, Indent: Left: 0 cm, Right: 0 cm, Line spacing: 1.5 lines

93

94 Several studies have investigated the North Pacific influence on the tropics using surface flux-

95 restoring in a model (Alexander et al. 2010; Sun and Okumura 2019; Liu et al. 2021). Alexander

96 et al. (2010) and Sun and Okumura (2019) imposed surface flux anomalies derived from the North

97 Pacific Oscillation (NPO) - the anomalous North Pacific pattern projecting onto the second EOF of

Formatted: Justified, Space After: 0 pt, Line spacing: 1.5 lines

Formatted: Justified, Indent: Left: 0 cm, Right: 0 cm, Line spacing: 1.5 lines

Formatted: Header

low frequency tropical Pacific SST variability. They showed that surface forcing associated with the NPO can affect decadal variability in the tropics. The proposed mechanism for ~~communication~~ ~~of communicating~~ extratropical surface anomalies ~~inteto~~ the tropics is the seasonal footprinting mechanism (SFM) (Alexander et al. 2010; Sun and Okumura 2019; Amaya et al. 2019, Liu et al. 2021). Atmospheric circulation anomalies driven by the subtropical portion of the high latitude SST footprint modulate tropical SSTs through coupled atmosphere-ocean processes, leading to anomalies that persist through boreal spring-summer. However, the amplitude of the effect on tropical Pacific SSTs from the North Pacific has been suggested to be quite weak on decadal timescales (Alexander et al. 2010; Sun and Okumura 2019; Liguori and Di Lorenzo 2019). Moreover, the studies did not directly isolate driving by the Aleutian Low, which has been highlighted in studies arguing a role for anthropogenic forcing of recent observed PDO variability (Smith et al. 2016; Klavans et al. submitted).

Formatted: Justified, Space After: 0 pt, Line spacing: 1.5 lines

In this study, we aim to better understand the role of long-term changes in the Aleutian Low in governing the multi-annual behaviour of tropical Pacific SSTs. We perform an ensemble of atmospheric nudging simulations in an intermediate complexity coupled climate model to isolate the effect of ~~an anomalous sustained anomaly in the~~ Aleutian Low ~~and compare~~. ~~The response to this with regional perturbation is compared to the~~ internally-generated low frequency Pacific variability in a free running simulation. The manuscript is structured as follows: section 2 describes the methodology and details of the model used. Section 3 compares the results of the nudging simulations with the free running simulation. Discussion of the results is provided in section 4 and conclusions in section 5.

Formatted: Justified, Indent: Left: 0 cm, Right: 0 cm, Line spacing: 1.5 lines

## 2. Data and Methods

Formatted: Normal, Justified, Indent: Left: 0 cm, First line: 0 cm, Line spacing: 1.5 lines

Formatted: Font: 11 pt, Bold

### 2.1 FORTE 2.0

Formatted: Font: Bold

Formatted: Font: 11 pt, Bold

Formatted: Font: Bold

Formatted: Normal, Justified, Indent: Left: 0 cm, First line: 0 cm, Line spacing: 1.5 lines

130 Simulations were performed using FORTE2.0, an intermediate complexity coupled  
 131 ~~AtmosphereOcean~~Atmosphere-Ocean General Circulation Model (AOGCM) (Blaker et al., 2021).  
 132 The atmospheric model IGCM4 (Intermediate General Circulation Model 4) (Joshi et al., 2015)  
 133 uses a truncated series of spherical harmonics run at T42 resolution with 20  $\sigma$ -levels to a height  
 134 of  $\sigma = 0.05$ . IGCM4 is coupled to the MOMA (Modular Ocean Model – Array) (Webb, 1996) ocean  
 135 model run at  $2^\circ \times 2^\circ$  resolution with 15 vertical levels. The two components are coupled once per  
 136 day using OASIS version 2.3 (Terry et al., 1999) and PVM version 3.4.6 (Parallel Virtual  
 137 Machine). As described in Blaker et al. (2021), between  $5^\circ$  N/S and the equator the horizontal  
 138 ocean diffusion increases by a factor of 20 to balance equatorial upwelling and parameterise the  
 139 eddy heat convergence. For more details on the model see Blaker et al. (2021). The model  
 140 simulates ~~low frequency~~multi-decadal SST variability in the Pacific with a similar pattern to that  
 141 seen in observations but a weaker amplitude by around a factor of 4 to 5 (Figure S1).

## 2.2 Grid-point nudging method

146 Atmospheric nudging has been used to investigate climate and weather relationships between  
 147 remote phenomena (e.g. Martin et al., 2021; Knight et al., 2017; Watson et al., 2016). A nudging  
 148 code was added to IGCM4. Nudging was performed by adding tendencies to horizontal winds,  
 149 temperature and surface pressure. The nudging code is publicly available at  
 150 (<https://github.com/NOC-MSM/FORTE2.0>~~https://github.com/NOC-MSM/FORTE2.0~~).

151 The nudging configuration is similar to that in Watson et al. (2016), with two additional terms to  
 152 account for vertical (z) and temporal (t) variation in the nudging strength:

$$\delta x(\lambda, \phi, z, t) = -\gamma(\lambda, \phi, z, t)(x(\lambda, \phi, z, t) - x_{ref}(\lambda, \phi, z, t))/\tau, \quad (\text{Eqn 1})$$

$$\delta x(\lambda, \phi, z, t) = -\gamma(\lambda, \phi, z, t)(x(\lambda, \phi, z, t) - x_{ref}(\lambda, \phi, z, t))/\tau, \quad (\text{Eqn 1})$$

155 where  $x$  is the variable being relaxed as a function of longitude ( $\lambda$ ) and latitude ( $\phi$ ),  $x_{ref}$  is the  
 156 reference state, and  $\tau$  is the nudging strength (set to 6hr). The spatial extent of  
 157 the nudging was tested extensively to avoid any shock at the boundaries and spurious effects of  
 158 nudging near polar regions. The regional extent was determined as:

$$\gamma(\phi, \lambda) = f(\phi, \phi_1, \phi_2)f(\lambda, \lambda_1, \lambda_2), \quad (\text{Eqn 2})$$

Formatted: Header

Formatted: Justified, Indent: Left: 0 cm, Right: 0 cm, Space Before: 12 pt, Line spacing: 1.5 lines

Formatted: Pattern: Clear (White)

Formatted: Pattern: Clear (White)

Formatted: Normal, Justified, Indent: Left: 0 cm, First line: 1.27 cm, Line spacing: 1.5 lines

Formatted: Font: 11 pt, Bold

Formatted: Font: Bold

Formatted: Justified, Space After: 0 pt, Line spacing: 1.5 lines

Formatted: Justified, Indent: Left: 0 cm, Right: 0 cm, Space After: 0 pt, Line spacing: 1.5 lines

Formatted: Underline, Font color: Custom Color(RGB(17,85,204))

Formatted: Justified, Indent: Left: 0 cm, Right: 0 cm, Space Before: 12 pt, After: 0 pt, Line spacing: 1.5 lines

Formatted: Font: 11 pt, Subscript

Formatted: Header

$$\gamma(\phi, \lambda) = f(\phi, \phi_1, \phi_2)f(\lambda, \lambda_1, \lambda_2), \quad \text{(Eqn 2)}$$

where

$$f(\phi, \phi_1, \phi_2) = [1/(1 + e^{-(\phi - \phi_1)/\delta_1})][1 - 1/(1 + e^{-(\phi - \phi_2)/\delta_2})]f(\phi, \phi_1, \phi_2) = [1/(1 + e^{-(\phi - \phi_1)/\delta_1})][1 - 1/(1 + e^{-(\phi - \phi_2)/\delta_2})] \quad \text{(Eqn 3)}$$

and

$$f(\lambda, \lambda_1, \lambda_2) = [1/(1 + e^{-(\lambda - \lambda_1)/\delta_1})][1 - 1/(1 + e^{-(\lambda - \lambda_2)/\delta_2})] \quad \text{(Eqn 4)}$$

$\Phi_1 = 30^\circ\text{N}$  and  $\Phi_2 = 65^\circ\text{N}$  represent the southern and northern limits of the nudging region and  $\lambda_1 = 160^\circ\text{E}$  and  $\lambda_2 = 140^\circ\text{W}$  are the western and eastern limits of the nudging region. The horizontal limits follow the commonly defined North Pacific Index (NPI) (Trenberth and Hurrell, 1994) as a proxy for the region encompassed by the Aleutian Low.

The temporal and nudging variations are determined as:

$$f(z) = a \cdot \exp(bz) \quad \text{(Eqn 5)}$$

$$f(t) = \left( \frac{1}{\exp\left(-0.5 \cdot \left(\frac{d^2}{\beta^2}\right)^{2\mu}\right)} \right) \quad \text{(Eqn 6)}$$

The strength of the tropospheric nudging is set to 1 (constant  $a$ , Equation 5) at  $\xi = 0.96$  (lowest atmospheric level), decreasing exponentially to 0 at  $\xi = 0.05$  (tropopause) (Equation 5). Nudging is applied during the extended boreal winter season (NDJFM) peaking on 15 January, with a Gaussian function in time to increase the nudging strength from 0 to 1 between 1 to 30 November and a reverse ramp-down during March. Term  $d$  (Equation 6) is the day within the nudging period.  $\beta$  is a constant set to 1.2.  $\mu$  is a constant set to 2. The spatio-temporal forms of the nudging coefficients are shown in Figure S2.

The strong Aleutian Low state is taken from a 100 year long control run (CONTROL) based on a winter month with an NPI anomaly of  $-3.02\sigma$ , ( $-10.76$  hPa), where  $\sigma$  is the standard deviation calculated over all winter months in CONTROL. (Figure S3). Therefore, the target state represents

Formatted: Justified, Indent: Left: 0 cm, Right: 0 cm, Space Before: 12 pt, After: 0 pt, Line spacing: 1.5 lines

Formatted: Justified, Indent: Left: 0 cm, First line: 0 cm, Right: 0 cm, Space Before: 12 pt, Line spacing: 1.5 lines

Formatted: Justified, Indent: Left: 0 cm, Space Before: 12 pt, After: 0 pt, Line spacing: 1.5 lines, Tab stops: Not at 1.27 cm + 8.57 cm

Formatted: Justified, Indent: Left: 0 cm, Right: 0 cm, Space Before: 12 pt, After: 0 pt, Line spacing: 1.5 lines

Formatted: Pattern: Clear (White)

Formatted: Pattern: Clear (White)

Formatted: Font: Arial

Formatted: Font: Arial

Formatted: Header

185 an extreme intense Aleutian Low state as simulated in FORTE2.0. ~~Comparing with ERA5~~  
186 ~~reanalysis data from 1979-2020, the most intense winter month has an NPI anomaly of -3.56 (-~~  
187 ~~18.13 hPa). The imposed atmospheric forcing is therefore weaker than if an equivalent experiment~~  
188 ~~was conducted using reanalysis data.~~  $x_{ref}$  comprises the anomaly of ~~this~~ the chosen month added  
189 to the daily climatology. A 50 member NUDGED ensemble was generated using initial conditions  
190 drawn from each January 1<sup>st</sup> of the final 50 years of CONTROL. Each member is integrated for 30  
191 years with nudging commencing on 1 November of the first year and repeating each winter of the  
192 simulation. Unless otherwise stated, the analysis shows ensemble mean anomalies in the  
193 NUDGED simulation compared to the long-term climatology of CONTROL. Statistical significance  
194 is defined by comparing the responses to the magnitude of ~~internal variability.~~ ~~For CONTROL,~~  
195 ~~variability is calculated by multiplying the standard deviation of overlapping 15-year means by  $\sqrt{2}$ .~~  
196 ~~simulated unforced decadal variability. At each grid point, overlapping 15-year mean anomalies~~  
197 ~~are calculated from CONTROL. A 15-year time window was chosen to adequately capture decadal~~  
198 ~~internal variability. The standard deviation of the mean anomalies from CONTROL was multiplied~~  
199 ~~by square root of 2 to account for the fact that the variability of a difference in means is of interest.~~  
200 ~~This estimates the variation of the difference in standard deviation between two independent~~  
201 ~~averages, which have the same variance, that would be expected due to internal variability. The~~  
202 ~~median value of the standard deviations is used and we show 95% significance as where the~~  
203 ~~response value lies outside of the bounds 1.96 times the median standard deviation. This is similar~~  
204 ~~to the method used in IPCC AR5 (2013).~~

Formatted: Font: ArialMT

205 ~~The median value of the standard deviation is used and the result is statistically significant at the~~  
206 ~~95% level if the ensemble mean response lies outside of the bounds  $\pm 1.96 \times SD$ .~~

### 209 **2.3 Mixed Layer Heat Budget Analysis**

Formatted: Font: 11 pt, Bold

210 The heat budget of the upper ~~30m of the~~ ocean (representing the mixed layer (assumed to be 30  
211 ~~m deep)~~ is analysed for the regions shown by the boxes in Figure 1, where the temperature  
212 tendency is given by:  ~~$\frac{dT}{dt} = ADV + DIFF_{vert} + DIFF_{horiz} + CONV$  (Eqn. 5).~~

Formatted: Font: Bold

Formatted: Normal, Justified, Indent: Left: 0 cm, First line: 1.27 cm, Space Before: 12 pt, After: 0 pt, Line spacing: 1.5 lines

$$\frac{dT}{dt} = ADV + DIFF_{vert} + DIFF_{horiz} + CONV \text{ (Eqn. 7)}$$



Formatted: Header

214 Daily tendencies due to advection (ADV), vertical and horizontal diffusion ( $DIFF_{\text{vert}}$  and  $DIFF_{\text{horiz}}$ )  
215 and convection (CONV) are output from the model. [Further granularity in the heat budget terms](#)  
216 [\(e.g. turbulent fluxes\) was not possible due to the limited availability of diagnostics from the](#)  
217 [model.](#) Vertical diffusion represents the contribution to the mixed layer heat budget from surface  
218 turbulent and radiative fluxes. ADV is composed of zonal, meridional and vertical components:

$$219 \text{-----} \frac{\delta T}{\delta x} \text{-----} \frac{\delta T}{\delta y} \text{-----} \frac{\delta T}{\delta z} \text{-----}$$
$$220 \text{-----} ADV = u \frac{\delta T}{\delta x} + v \frac{\delta T}{\delta y} + w \frac{\delta T}{\delta z} \text{-----} \text{ (Eqn. 6),}$$
$$221 \text{-----}$$

$$222 \text{-----} ADV = u \frac{\delta T}{\delta x} + v \frac{\delta T}{\delta y} + w \frac{\delta T}{\delta z} \text{-----}$$

223 [\(Eqn. 8\)](#)

224 where u, v and w are the zonal, meridional and vertical components of the ocean velocity and  
225  $dT/dx$  represents the local zonal gradient of temperature. We linearize the meridional advection  
226 term to investigate the relative roles of changes to ocean current velocity and temperature gradient  
227 as follows:

$$228 \text{-----} \frac{\delta T}{\delta y} \text{-----} \frac{\delta T^0}{\delta y} \text{-----} \frac{\delta T}{\delta y} \text{-----} \frac{\delta T}{\delta y} \text{-----}$$
$$229 \text{-----} (v \frac{\delta T}{\delta y})' = v' \frac{\delta T}{\delta y} + v_0 (\frac{\delta T}{\delta y})' + v' (\frac{\delta T}{\delta y})' \text{-----} \text{ (Eqn. 7)}$$

$$230 \text{-----} (v \frac{\delta T}{\delta y})' = v' \frac{\delta T_0}{\delta y} + v_0 (\frac{\delta T}{\delta y})' + v' (\frac{\delta T}{\delta y})' \text{-----} \text{ (Eqn. 9)}$$

231 where the subscript 0 denotes CONTROL values and primes denote anomalies in NUDGED.

## 232 [2.4 PDO Index](#)

233 The PDO index is calculated as the first EOF of monthly SST anomalies, calculated as deviations  
234 from the climatological seasonal cycle, over the region 20-65°N, 120-260°E. [\(Mantua et al. 1997\).](#)  
235 Before calculating the leading EOF, the temperature anomalies are weighted by the square-root  
236 of the cosine of latitude to account for the decrease in area towards the pole. The monthly principal  
237 component, corresponding to the PDO index, is normalised by the standard deviation to give it  
238 unit variance. The pattern of temperature anomalies that covaries with the PDO is found by linearly  
239 regressing the time series of the monthly mean temperature anomalies onto the monthly PDO  
240 index (Figure 1b). [Here we define the PDO using the common index based on the leading EOF of](#)  
241 [North Pacific SST variability. Wills et al. \(2019\) showed that the tropical Pacific SST anomalies](#)  
242 [associated with this index are predominantly related to high frequency \(e.g., ENSO\) SST](#)  
243 [variability, while the extratropical part is related to turbulent heat flux and wind stress anomalies](#)

Formatted: Justified, Indent: Left: 0 cm, Right: 0 cm,  
Space Before: 12 pt, After: 0 pt, Line spacing: 1.5 lines

Formatted: Justified, Indent: Left: 0 cm, Right: 0 cm,  
Space Before: 12 pt, Line spacing: 1.5 lines

Formatted: Justified, Indent: Left: 0 cm, Right: 0 cm,  
Space Before: 12 pt, After: 0 pt, Line spacing: 1.5 lines

Formatted: Font: 11 pt, Bold

244 associated with intrinsic Aleutian Low variability. The discrepancy between the modelled and  
245 observed SST anomalies associated with the PDO index in Figure S1 could be due to the slightly  
246 weaker than observed ENSO amplitude in the model by around 33% (Figure S4) (see also Blaker  
247 et al., 2021).

Formatted: Header

Formatted: Font Italic, Font color: Blue

### 248 **3. Results**

Formatted: Font: 11 pt, Bold

Formatted: Font: Bold

#### 251 3.1 Surface temperature response

Formatted: Normal, Justified, Indent: Left: 0 cm, First line: 0 cm, Space After: 6 pt, Line spacing: 1.5 lines

Formatted: Font: Italic

Formatted: Font: Symbol

252 Figure 1a shows annual mean surface temperature anomalies in NUDGED expressed as a change  
253 per standard deviation ( $\sigma$ ) of the PDO index. A horse-shoe pattern of anomalous temperature  
254 extends across the North Pacific, comprising warming in the north and eastern Pacific and along  
255 the west coast of North America and cooling in the western North Pacific/KOE region. The  
256 strongest warming (0.2-0.3 K/ $\sigma$ ) is seen over the North Pacific and western North America. There  
257 is weaker (0.02-0.04 K/ $\sigma$ ) but statistically significant warming in the eastern and central equatorial  
258 Pacific. TheAcross the Pacific ocean, the pattern of temperature anomalies in NUDGED closely  
259 resembles unforced multidecadal Pacific variability in CONTROL (Figure 1b)-, with a pattern  
260 correlation coefficient of 0.53. Therefore, a sustained increase in Aleutian Low strength forces a  
261 basin-wide SST response thatwhich resembles internallygeneratedthat associated with internally-  
262 generated coupled variability in CONTROL. However, there are clear differences in the sign of the  
263 anomaly outside the North Pacific basin and nudging region, such as over north-eastern Siberia  
264 and south-central USA. Furthermore, while the extratropical SST anomalies are somewhat larger  
265 in NUDGED, particularly in the subpolar gyre, the tropical Pacific signal is substantially weaker by  
266 a factor of  $\sim 3$ . This indicates that atmospheric forcing by the Aleutian Low alone is not sufficient to  
267 generate a basin-wide SST response that is consistent with the intrinsic variability of the model.  
268 Note the Aleutian Low state in  $x_{ref}$  is extreme ( $-3\sigma$ ), meaning a more realistic amplitude for  
269 sustained Aleutian Low intensification can be expected to induce a weaker response.

Formatted: Font: Symbol

Formatted: Font: Symbol

Formatted: Font: Symbol

270 The seasonality of the surface temperature anomalies in NUDGED is shown in Figure 2 separated  
271 for years 1-2, years 3-4 and years 5-30. The initial response to the intensified Aleutian Low is a  
272 warming in the subpolar gyre in boreal autumn (SON). This amplifies in DJF during the peak of  
273 the nudging period, where a tongue of warming extends into the subtropical North Pacific. This  
274 pattern persists into MAM after nudging ceases but is also accompanied by warming in the eastern  
275 tropical Pacific. By JJA, the tropical and subtropical temperature changes have weakened leaving

Formatted: Header

276 residual warming in the subpolar gyre that persists into the following winter. The temperature  
277 anomalies over land quickly dissipate due to the low specific heat capacity. A similar seasonal  
278 evolution occurs in years 3-4, but the tropical warm anomaly emerges earlier in DJF and extends  
279 further westward at its peak in MAM. The anomalies in years 5-30 show a similar spatiotemporal  
280 pattern to the first 4 years, suggesting the mechanisms by which the anomalies manifest do not  
281 evolve strongly when the signals are maintained over multi-year timescales. Small differences  
282 between years 1-4 and 5-30 are the extent of the robust signal in the tropical Pacific; there is a  
283 small reduction in the amplitude of the tropical warming in JJA and no significant western tropical  
284 Pacific warming in MAM for years 5-30. The signal of peak tropical warming in MAM in NUDGED  
285 qualitatively agrees with observed low frequency Pacific variability (Figure S1), though we note  
286 that FORTE2.0 shows a narrower band of tropical warming compared to observations.  
287 Furthermore, the weak footprint of modelled PDO variability in the equatorial Pacific (Fig. S1) is  
288 consistent with a notion that Aleutian Low driven SST variability in the extra-tropics has little  
289 influence on tropical variability (Wills et al., 2019; Zhao et 2021).

290  
291

### 292 3.2 Mixed layer heat budget

293 The mixed layer heat budget in the subtropical North Pacific and Niño 3.4 regions shows different  
294 annual cycles in the anomalous temperature tendencies (Figure 3 a,b). The largest anomalous  
295 surface temperature tendency in the subtropical North Pacific occurs during the nudging period  
296 (DJF), whereas the peak warming tendency in the Niño3.4 region occurs in February-April. In the  
297 subtropics in winter, warming from vertical diffusion is offset by meridional advection. In contrast  
298 in the Niño 3.4 region, anomalous meridional advection contributes to a warming tendency  
299 ~~year-round~~ year-round, with the maximum (~0.3 K/month) in MAM. This warming is partly offset by  
300 anomalous vertical diffusion and convection. Meridional advection therefore contributes to cooling  
301 in the subtropical North Pacific but causes warming in the Niño 3.4 region.

302

303 The anomalous meridional advection in the subtropical North Pacific is dominated by the change  
304 in meridional velocity, whilst in the Niño3.4 region the change in meridional temperature gradient  
305 is the largest contributor throughout most of the year (apart from Sept-Dec). The enhanced  
306 warming tendency from Feb-June in the Niño3.4 region is driven by changes in meridional velocity.

Formatted: Normal, Justified, Indent: Left: 0 cm, First line: 0 cm, Space After: 6 pt, Line spacing: 1.5 lines

Formatted: Font: Italic

Formatted: Justified, Space After: 6 pt, Line spacing: 1.5 lines

Formatted: Justified, Indent: Left: 0 cm, Right: 0 cm, Space After: 6 pt, Line spacing: 1.5 lines

307 The difference in contributing terms implies different mechanisms governing the changing mixed  
308 layer temperatures in the two regions.

309  
310 The net surface heat flux anomalies in NUDGED are shown in Figure 4(a-d). There are positive  
311 net surface heat flux anomalies across the North Pacific and within a SW-NE oriented band in the  
312 subtropical North Pacific. The largest heat flux anomalies occur during DJF, with values in excess  
313 of  $4 \text{ W m}^{-2}/\sigma$ . The net surface heat flux anomalies in NUDGED are dominated by the latent heat  
314 flux (Fig. 4 e-h). The pattern of surface latent heat flux anomalies in JJA in the extratropical North  
315 Pacific resembles that for the internal PDO structure (Figure S34), with positive flux anomalies  
316 extending eastward from the KOE region, which are enveloped by negative anomalies in the  
317 northeast Pacific and subtropical North Pacific. ~~The~~The positive heat fluxes exhibited in the KOE  
318 region in all seasons outside of DJF are evidence that cold SST anomalies in this region reduce  
319 heat loss to the atmosphere throughout the simulations. Regions such as those in the north-east  
320 North Pacific appear to dampen the SST anomalies during MAM and JJA, which may indicate  
321 limited dynamic feedback to the atmosphere. However, across the central North Pacific, the  
322 persistence of surface latent flux anomalies year-round is expected given the surface temperature  
323 persistence and alludes to ~~oceanatmosphere~~ocean-atmosphere feedbacks.

### 326 3.3 Atmospheric circulation response

327 Figure 5 shows the seasonal mean zonal and meridional near-surface wind anomalies in  
328 NUDGED. As expected, the largest anomalies occur in the period over which nudging is applied  
329 (DJF), with a westerly zonal wind anomaly of up to  $\sim 0.5 \text{ ms}^{-1}/\sigma$  in the subtropics and an easterly  
330 anomaly of a similar magnitude in the subpolar extratropics. The meridional wind shows alternating  
331 southerly-northerly anomalies across the North Pacific orientated with a north-easterly tilt  
332 suggesting ~~a Rossby wave train response that a persistently strong AL invokes a modulation of~~  
333 the climatological Rossby wave train providing a pathway for atmospheric communication between  
334 the North Pacific and eastern tropical Pacific. Evidence for the modulation of the Rossby wave  
335 train is further evident in the upper tropospheric winds (Figure S5). The subtropical zonal wind  
336 anomalies project onto a southerly shift of the westerlies compared to the climatology in  
337 CONTROL, with persistent anomalies extending into the spring after nudging ceases (MAM).  
338 Interestingly, there is an emergence of a westerly wind anomaly near the coast of ~~California~~Central

Formatted: Header

Formatted: Justified, Space After: 6 pt, Line spacing: 1.5 lines

Formatted: Justified, Indent: Left: 0 cm, Right: 0 cm, Line spacing: 1.5 lines

Formatted: Font: Symbol

Formatted: Font color: Text 1

Formatted: Normal, Justified, Indent: Left: 0 cm, First line: 0 cm, Space After: 6 pt, Line spacing: 1.5 lines

Formatted: Font: Italic

Formatted: Font: Symbol

339 America in DJF that extends southward and westward into the equatorial Pacific in MAM. Although  
340 zonal wind anomalies are evident in JJA, they are not strongly statistically significant.

341 Figure 6 shows the latitude-time evolution of surface temperature, near-surface wind and surface  
342 pressure anomalies in NUDGED averaged over the central and eastern tropical Pacific. There is  
343 year-round warming in subtropical and equatorial regions, with the largest magnitude in the  
344 subtropics from November through April ( $-0.05 \text{ K}/\sigma$ ) and in the equatorial region from March  
345 through July ( $-0.3 \text{ K}/\sigma$ ). The nudging invokes concurrent warming in the subtropics, while there is  
346 a seasonal delay in the emergence of warming in the equatorial Pacific. From July to November  
347 in the subtropics (around  $15^\circ\text{N}$ ) there is substantially less warming than during the rest of the year,  
348 with values close to zero. The westerly wind anomalies coincide with the timing of the temperature  
349 anomalies, with south-westerly anomalies of  $-0.05 \text{ m s}^{-1}/\sigma$  in the subtropics and  $-0.03 \text{ m s}^{-1}/\sigma$  in  
350 the equatorial region. In addition to the cross-equatorial temperature gradient generated by the  
351 subtropical anomaly, the lower surface pressure in the northern subtropics ( $-1.5 \text{ hPa}$ ), which is  
352 largest in February and March, creates a pressure gradient across the equator-, a key component  
353 of the WES mechanism. At this time there is evidence of cooling in the southern subtropics (south  
354 of  $15^\circ\text{S}$ ).

#### 357 **4. Discussion**

358  
359 The impact of an intensified Aleutian Low on the tropical Pacific in this study suggests an excitation  
360 of the SFM mechanism (e.g. Vimont et al. 2003; Alexander et al. 2010; Chen and Yu, 2020; Sun  
361 and Okumura, 2019). In accordance with the SFM, the SST anomalies persist into the summer  
362 season, with anomalous temperatures found in the North Pacific year-round. The signals in winter  
363 and spring show a similar spatial signature to that found by Liguori and Di Lorenzo (2019), who  
364 show an SST signature in the subtropics as a precursor to ENSO dynamics. Here we find a similar  
365 effect on multi-year timescales in response to an anomalous Aleutian Low.

366  
367 The midlatitude westerly winds show a southerly shift throughout the year which, in agreement  
368 with Liu et al. (2021), acts to prevent heat loss from the surface due to reduced evaporation. This  
369 in turn drives the SST anomaly towards the equator. Liu et al. (2021) show the SFM as the  
370 mechanism that propagates SST anomalies southward, through a change in latent heat fluxes.  
371 However, in DJF the westerly winds imposed by the nudging cause a weakening of the subtropical

Formatted: Header

Formatted: Font: Symbol

Formatted: Font: Symbol

Formatted: Font: Symbol

Formatted: Font: Symbol

Formatted: Normal, Indent: Left: 0 cm, First line: 0 cm, Line spacing: 1.5 lines

Formatted: Font: 11 pt, Bold

Formatted: Font: Bold

Formatted: Space After: 0 pt, Line spacing: 1.5 lines

Formatted: Font: Bold

Formatted: Justified, Indent: Left: 0 cm, Right: 0 cm, Line spacing: 1.5 lines

Formatted: Justified, Space After: 0 pt, Line spacing: 1.5 lines

Formatted: Justified, Indent: Left: 0 cm, Right: 0 cm, Line spacing: 1.5 lines

Formatted: Header

372 trades; hence the southerly shift of westerlies starts to occur within the season of nudging. We  
373 show anomalous latent heat flux is responsible for the change in subtropical North Pacific SSTs.  
374 The limitation of the Liu et al. (2021) study is that the atmosphere was coupled to a thermodynamic  
375 slab-ocean, whereas we integrate a fully coupled ocean model allowing for a role of ocean  
376 dynamical feedbacks. Sun and Okumura (2019) conducted a related investigation by imposing  
377 heat flux anomalies associated with the North Pacific Oscillation, (NPO), which is a coupled  
378 ~~atmosphereocean~~atmosphere-ocean mode, but they imposed a fixed year round anomaly  
379 whereas the Aleutian Low shows strongest variability in winter and therefore we only impose  
380 relaxation during boreal winter in our experimental design. The simulations presented use an  
381 anomalous Aleutian Low state taken from a single month (Figure S3). An area for future research  
382 is to impose a suite of varying Aleutian Low states with different spatial and temporal profiles to  
383 test the sensitivity of the responses described here to details of the imposed relaxation state.

Formatted: Font: Italic, Font color: Blue

Formatted: Justified, Line spacing: 1.5 lines

385 In the tropical Pacific, the dominant mechanism responsible for the increase in SSTs is meridional  
386 advection, with the change to meridional current velocity driving the accelerated warming in boreal  
387 spring. This coincides with a northward cross-equatorial SST gradient and the development of an  
388 anomalous cross-equatorial southward pressure gradient. Cross-equatorial winds are generated,  
389 which, due to Coriolis force act to weaken the trades in the northern equatorial region, decreasing  
390 the surface latent heat flux and leading to a local warming. The heat budget analysis shows that  
391 surface heat fluxes are the primary warming agent during the nudging period, whereas a change  
392 to surface advection drives the warming in the central tropical Pacific. A comprehensive review of  
393 this mechanism, commonly referred to as the wind-evaporation-SST (WES) mechanism, is  
394 provided in Mahajan et al. (2008). Further, the mechanism has been posited as a pathway through  
395 which North Pacific SSTs can influence ENSO variability (Amaya et al. 2019). Investigation into  
396 equatorial thermocline depth shows a slight deepening of the thermocline in all seasons apart from  
397 SON, which is supported by changes in the vertical advection term (not shown). Figure 7 gives a  
398 pictorial representation of the combined mechanisms involved in translating the Aleutian Low  
399 anomaly into the deep tropics.

Formatted: Justified, Indent: Left: 0 cm, Right: 0 cm,  
Line spacing: 1.5 lines

400  
401 While the results make conceptual sense and are in broad agreement with studies using more  
402 comprehensive modelling tools (see earlier references), the amplitude of the response could be  
403 verified in other more detailed coupled climate models. The coarseness of the coupled model,  
404 specifically the vertical dimension of the oceanic component, is a limitation of the study.  
405 Specifically, the model's relatively low resolution and inability to resolve mesoscale processes in

Formatted: Justified, Space After: 0 pt, Line spacing:  
1.5 lines

Formatted: Justified, Indent: Left: 0 cm, Right: 0 cm,  
Line spacing: 1.5 lines

406 [the ocean and atmosphere may affect the results of the study. Future studies using observations](#)  
407 [and higher resolution GCMs to test the results herein would be valuable. Furthermore, to ensure](#)  
408 [model stability, the anomalous nudging state was drawn from the coupled atmosphere-ocean](#)  
409 [control simulation. The Aleutian Low variability sampled from this simulation therefore includes](#)  
410 [effects from tropical variability. The month used as the reference state for the nudging coincides](#)  
411 [with an ENSO state \(magnitude = 0.55\) in the tropical Pacific. Further study could investigate more](#)  
412 [idealised AL states and their effects on extra-tropical-tropical communication.](#)

Formatted: Header

## 415 5. Conclusions

Formatted: Font color: Red

416 Externally-forced Aleutian Low trends have been implicated as a potential driver of recent  
417 variations in the Pacific Decadal Oscillation (Smith et al., 2016; Klavans et al., submitted). Here,  
418 we have investigated the potential influence of Aleutian Low trends on basin-wide low frequency  
419 Pacific sea surface temperature variability using nudging simulations in an intermediate complexity  
420 climate model. The target Aleutian Low state represents an extremely intense Aleutian Low state  
421 (-3 $\sigma$  of winter monthly variability) applied during boreal winter. The intensified Aleutian Low  
422 induces a basin-wide SST response that resembles the model's internally-generated PDO with a  
423 comparable amplitude in the extratropics, but a substantially weaker amplitude in the equatorial  
424 Pacific by a factor of 4 to 5. [The pattern of SST variability exhibited across the basin is evident on](#)  
425 [interannual timescales as well as throughout the duration of the 30 year simulation.](#)

Formatted: Normal, Indent: Left: 0 cm, First line: 0 cm, Line spacing: 1.5 lines

Formatted: Font: 11 pt, Bold

Formatted: Space After: 0 pt, Line spacing: 1.5 lines

Formatted: Justified, Indent: Left: 0 cm, Right: 0 cm, Line spacing: 1.5 lines

426 The findings presented here support that the PDO can, at least in part, be driven by remotely  
427 forced changes in the North Pacific atmospheric circulation independent of the tropics. However,  
428 in our experiment the amplitude appears to be too weak to fully explain a multi-annual shift in the  
429 PDO: [across the tropics](#). This suggests that the hypothesis posed by Smith et al. (2016) and  
430 Klavans et al. (submitted), that anthropogenically forced changes in the Aleutian Low drove the  
431 observed shift in the phase of the [basin-wide](#) PDO in the late 20th and early 21st centuries, should  
432 be revisited.

Formatted: Font: Symbol

Formatted: Justified, Space After: 0 pt, Line spacing: 1.5 lines

Formatted: Justified, Indent: Left: 0 cm, Right: 0 cm, Line spacing: 1.5 lines, Pattern: Clear (Background 1)

Formatted: Justified, Space After: 0 pt, Line spacing: 1.5 lines

Formatted: Font: Bold, Underline

Formatted: Font: 11 pt, Bold

Formatted: Normal, Justified, Indent: Left: 0 cm, Line spacing: 1.5 lines

Formatted: Font: Bold

Formatted: Font: Bold

## 436 Code availability

Formatted: Justified, Space After: 0 pt, Line spacing: 1.5 lines

437 The nudging code used in the analysis can be found:  
438 [\(\(https://github.com/NOC-MSM/FORTE2.0](https://github.com/NOC-MSM/FORTE2.0)  
439 [https://github.com/NOC-MSM/FORTE2.0\)](https://github.com/NOC-MSM/FORTE2.0)

Formatted: Justified, Indent: Left: 0 cm, Right: 0 cm, Space After: 0 pt, Line spacing: 1.5 lines

Formatted: Underline, Font color: Custom Color(17,85,204)

440  
 441 ).  
 442  
 443 **Data availability**  
 444  
 445 Underlying model data found in this paper is available from the corresponding author upon request.  
 446  
 447 HadISST data available: <https://www.metoffice.gov.uk/hadobs/hadisst/data/download.html>  
 448  
 449  
 450 [HadISST data available: https://www.metoffice.gov.uk/hadobs/hadisst/data/download.html](https://www.metoffice.gov.uk/hadobs/hadisst/data/download.html)  
 451  
 452 **Author contribution**  
 453  
 454  
 455 WJD and ACM designed the study. WJD developed the nudging code in FORTE2.0 with support  
 456 from CMM, MMJ and RR. ATB and RR helped with installation of FORTE2.0 at Leeds. WJD  
 457 performed the analysis and produced the figures. WJD and ACM wrote the manuscript with  
 458 comments from all authors. All simulations were performed on the ARC4 HPC at the University of  
 459 Leeds.  
 460  
 461 **Competing interests**  
 462  
 463 The authors declare that they have no conflict of interest.  
 464  
 465 **Acknowledgements**  
 466  
 467 WJD was supported by a Natural Environment Research Council (NERC) Ph.D. studentship  
 468 through the SPHERES Doctoral Training Partnership (NE/L002574/1) and by a Met Office  
 469 CASE studentship. ACM and CMM were supported by the European Union's Horizon 2020  
 470 Research and Innovation Programme under Grant Agreement 820829 (CONSTRAIN project).  
 471 ACM was supported by the Leverhulme Trust. We are grateful to Paloma Trascasa-Castro for  
 472 discussion of  
 473 ENSO processes. We are grateful for feedback on an earlier version of this manuscript from John  
 474 Marsham and Laura Wilcox.

- Formatted: Header
- Formatted: Font: 11 pt, Bold
- Formatted: Font: Bold
- Formatted: Normal, Justified, Indent: Left: 0 cm, Line spacing: 1.5 lines
- Formatted: Justified, Space After: 0 pt, Line spacing: 1.5 lines
- Formatted: Font: Bold
- Formatted: Justified, Indent: Left: 0 cm, Right: 0 cm, Line spacing: 1.5 lines
- Formatted: Font: 11 pt, Bold
- Formatted: Normal, Justified, Indent: Left: 0 cm, Line spacing: 1.5 lines
- Formatted: Font: Bold
- Formatted: Justified, Indent: Left: 0 cm, Right: 0 cm, Line spacing: 1.5 lines
- Formatted: Justified, Space After: 0 pt, Line spacing: 1.5 lines
- Formatted: Font: Bold
- Formatted: Justified, Indent: Left: 0 cm, Space After: 0 pt, Line spacing: 1.5 lines
- Formatted: Font: Bold
- Formatted: Justified, Space After: 0 pt, Line spacing: 1.5 lines
- Formatted: Font: Bold
- Formatted: Justified, Indent: Left: 0 cm, Right: 0 cm, Space After: 0 pt, Line spacing: 1.5 lines
- Formatted: Justified, Space After: 0 pt, Line spacing: 1.5 lines
- Formatted: Font: Bold, Underline
- Formatted: Font: 11 pt, Bold
- Formatted: Normal, Justified, Indent: Left: 0 cm, Line spacing: 1.5 lines
- Formatted: Font: Bold
- Formatted: Justified, Space After: 0 pt, Line spacing: 1.5 lines
- Formatted: Font: Bold, Underline
- Formatted: Justified, Indent: Left: 0 cm, Right: 0 cm, Line spacing: 1.5 lines



475  
476 **References**  
477

478 Alexander, M. A., & Deser, C. (1995). A mechanism for the recurrence of wintertime  
479 midlatitude SST anomalies. *Journal of Physical Oceanography*, 25(1), 122–137.  
480 [https://doi.org/10.1175/1520-0485\(1995\)025<0122:AMFTRO>2.0.CO;2](https://doi.org/10.1175/1520-0485(1995)025<0122:AMFTRO>2.0.CO;2)

481 Alexander, M. A., Vimont, D. J., Chang, P., & Scott, J. D. (2010). The impact of extratropical  
482 atmospheric variability on ENSO: Testing the seasonal footprinting mechanism using  
483 coupled model experiments. *Journal of Climate*, 23(11), 2885–2901.  
484 <https://doi.org/10.1175/2010JCLI3205.1>  
485 ~~2901. <https://doi.org/10.1175/2010JCLI3205.1>~~

486 Amaya, D. J., Kosaka, Y., Zhou, W., Zhang, Y., Xie, S. P., & Miller, A. J. (2019). The North  
487 Pacific pacemaker effect on historical ENSO and its mechanisms. *Journal of Climate*,  
488 32(22), 7643–7661. <https://doi.org/10.1175/JCLI-D-19-0040.1>

489 Barnett, T. P., Pierce, D. W., & Planck, M. (1999). Interdecadal interactions between the  
490 tropics and midlatitudes in the Pacific basin. *Geophysical Research Letters*, 26(5),  
491 615–618.

492 Blaker, A., Joshi, M., Sinha, B., Stevens, D., Smith, R., & Hirschi, J. (2021). FORTE 2.0: a  
493 fast, parallel and flexible coupled climate model. *Geoscientific Model Development*,  
494 ~~275–293. <https://doi.org/10.5194/gmd-14-275-2021>~~  
495 ~~275–293. <https://doi.org/10.5194/gmd-14-275-2021>~~

496 Chen, S., & Yu, B. (2020). The seasonal footprinting mechanism in large ensemble  
497 simulations of the second generation Canadian earth system model: uncertainty due to  
498 internal climate variability. *Climate Dynamics*, 55(9–10), 2523–2541.  
499 <https://doi.org/10.1007/s00382-020-05396-y>

500 Clement, A., DiNezio, P., & Deser, C. (2011). Rethinking the ocean's role in the Southern  
501 Oscillation. *Journal of Climate*, 24(15), 4056–4072.  
502 <https://doi.org/10.1175/2011JCLI3973.1>

Formatted: Header

Formatted: Space After: 0 pt, Line spacing: 1.5 lines

Formatted: Font: 11 pt, Bold

Formatted: Normal, Indent: Left: 0 cm, Line spacing: 1.5 lines

Formatted: Font: Bold

Formatted: Space After: 0 pt, Line spacing: 1.5 lines

Formatted: Indent: Left: 0.85 cm, Hanging: 0.85 cm, Right: 0 cm, Space Before: 12 pt, After: 12 pt, Line spacing: 1.5 lines

Formatted: Indent: Left: 0.85 cm, Hanging: 0.85 cm, Right: 0 cm, Space Before: 12 pt, After: 12 pt, Line spacing: 1.5 lines

Formatted: Indent: Left: 0.85 cm, Hanging: 0.85 cm, Right: 0 cm, Space Before: 12 pt, After: 12 pt, Line spacing: 1.5 lines

503  
504  
505  
506  
507  
508  
509  
510  
511  
512  
513  
514  
515  
516  
517  
518  
519  
520  
521  
522  
523  
524  
525  
526  
527  
528  
529

<https://doi.org/10.1175/2011JCLI3973.4>

Czaja, A., van der Vaart, P., & Marshall, J. (2002). A diagnostic study of the role of remote forcing in tropical Atlantic variability. *Journal of Climate*, 15(22), 3280–3290.

[https://doi.org/10.1175/1520-0442\(2002\)015<3280:ADSOTR>2.0.CO;2](https://doi.org/10.1175/1520-0442(2002)015<3280:ADSOTR>2.0.CO;2)

[https://doi.org/10.1175/1520-0442\(2002\)015<3280:ADSOTR>2.0.CO;2](https://doi.org/10.1175/1520-0442(2002)015<3280:ADSOTR>2.0.CO;2)

Deser, C., Sun, L., Tomas, R. A., & Screen, J. (2016). Does ocean coupling matter for the northern extratropical response to projected Arctic sea ice loss? *Geophysical Research Letters*, 43(5), 2149–2157. <https://doi.org/10.1002/2016GL067792>

Dittus, A. J., Hawkins, E., Robson, J. I., Smith, D. M., & Wilcox, L. J. (2021). Drivers of Recent North Pacific Decadal Variability: The Role of Aerosol Forcing. *Earth's Future*, 9(12). <https://doi.org/10.1029/2021EF002249>

Dow, W. J., Maycock, A. C., Lofverstrom, M., & Smith, C. J. (2021). The effect of anthropogenic aerosols on the aleutian low. *Journal of Climate*, 34(5), 1725–1741.

<https://doi.org/10.1175/JCLI-D-20-0423.1> <https://doi.org/10.1175/JCLI-D-20-0423.1>

[Gan, B. L. Wu, F. Jia, S. Li, W. Cai, H. Nakamura, M. A. Alexander, and A. J. Miller, 2017: On the response of the Aleutian Low to greenhouse warming. \*J. Climate\*, 30, 3907-3925, doi: 10.1175/JCLI-D-15-0789.1](#)

Gu, D., & Philander, S. G. H. (1997). Interdecadal climate fluctuations that depend on exchanges between the tropics and extratropics. *Science*, 275(5301), 805–807.

<https://doi.org/10.1126/science.275.5301.805>

Hu, D., & Guan, Z. (2018). Decadal relationship between the stratospheric arctic vortex and pacific decadal oscillation. *Journal of Climate*, 31(9), 3371–3386.

<https://doi.org/10.1175/JCLI-D-17-0266.1>

Jin, F. F. (2001). Low-frequency modes of tropical ocean dynamics. *Journal of Climate*, 14(18), 3874–3881. [https://doi.org/10.1175/1520-0442\(2001\)014<3874:LFMOTO>2.0.CO;2](https://doi.org/10.1175/1520-0442(2001)014<3874:LFMOTO>2.0.CO;2)

[https://doi.org/10.1175/1520-0442\(2001\)014<3874:LFMOTO>2.0.CO;2](https://doi.org/10.1175/1520-0442(2001)014<3874:LFMOTO>2.0.CO;2)

[https://doi.org/10.1175/1520-0442\(2001\)014<3874:LFMOTO>2.0.CO;2](https://doi.org/10.1175/1520-0442(2001)014<3874:LFMOTO>2.0.CO;2)

Formatted: Header

Formatted: Indent: Left: 0.85 cm, Right: 0 cm, Space Before: 12 pt, After: 12 pt, Line spacing: 1.5 lines

Formatted: Indent: Left: 0.85 cm, Right: 0 cm, Space Before: 12 pt, After: 12 pt, Line spacing: 1.5 lines

Formatted: Indent: Left: 0.85 cm, Hanging: 0.85 cm, Right: 0 cm, Space Before: 12 pt, After: 12 pt, Line spacing: 1.5 lines

Formatted: Indent: Left: 0.85 cm, Right: 0 cm, Space Before: 12 pt, Line spacing: 1.5 lines

Formatted: Indent: Left: 0.85 cm, Hanging: 0.85 cm, Right: 0 cm, Space Before: 12 pt, After: 12 pt, Line spacing: 1.5 lines

530 [Joshi, M., Hall, R. A., Stevens, D. P., and Hawkins, E.: The modelled climatic response](#)  
531 [to the 18.6-year lunar nodal cycle and its role in decadal temperature trends. \*Earth\*](#)  
532 [Syst. Dynam., 14, 443–455. <https://doi.org/10.5194/esd-14-443-2023>, 2023.](#)

533 Joshi, M., Stringer, M., Van Der Wiel, K., O’Callaghan, A., & Fueglistaler, S. (2015).  
534 IGCM4: A fast, parallel and flexible intermediate climate model. *Geoscientific Model*  
535 *Development*, 8(4), 1157–1167. <https://doi.org/10.5194/gmd-8-1157-2015>  
536 <https://doi.org/10.5194/gmd-8-1157-2015>

537 Klavans et al. (2023) [Recent Atlantic multidecadal variability and its impacts are driven by](#)  
538 [external forcings, external forcings, submitted](#)  
539 [, submitted](#)

540 Knight, J. R., Maidens, A., Watson, P. A. G., Andrews, M., Belcher, S., Brunet, G.,  
541 Fereday, D., Folland, C. K., Scaife, A. A., & Slingo, J. (2017). Global meteorological  
542 influences on the record UK rainfall of winter 2013–14. *Environmental Research*  
543 *Letters*, 12(7). <https://doi.org/10.1088/1748-9326/aa693c>

544 Knutson, T. R., & Manabe, S. (1998). Model assessment of decadal variability and trends in  
545 the tropical Pacific Ocean. In *Journal of Climate* (Vol. 11, Issue 9).  
546 [https://doi.org/10.1175/1520-0442\(1998\)011<2273:MAODVA>2.0.CO;2](https://doi.org/10.1175/1520-0442(1998)011<2273:MAODVA>2.0.CO;2)  
547 ~~[https://doi.org/10.1175/1520-0442\(1998\)011<2273:MAODVA>2.0.CO;2](https://doi.org/10.1175/1520-0442(1998)011<2273:MAODVA>2.0.CO;2)~~

548 Kwon, Y. O., & Deser, C. (2007). North Pacific decadal variability in the community climate  
549 system model version 2. *Journal of Climate*, 20(11), 2416–2433.  
550 <https://doi.org/10.1175/JCLI4103.1>

551 Latif, M., & Barnett, T. P. (1996). Decadal climate variability over the North Pacific and  
552 North America: Dynamics and predictability. *Journal of Climate*, 9(10), 2407–2423.  
553 [https://doi.org/10.1175/1520-0442\(1996\)009<2407:DCVOTN>2.0.CO;2](https://doi.org/10.1175/1520-0442(1996)009<2407:DCVOTN>2.0.CO;2)

554 Liguori, G., & Di Lorenzo, E. (2019). Separating the North and South Pacific Meridional  
555 Modes Contributions to ENSO and Tropical Decadal Variability. *Geophysical Research*  
556 *Letters*, 46(2), 906–915. <https://doi.org/10.1029/2018GL080320>

Formatted: Header

Formatted: Indent: Left: 0.85 cm, Hanging: 0.85 cm, Right: 0 cm, Space Before: 12 pt, Line spacing: 1.5 lines

Formatted: Hyperlink, No underline, Underline color: Auto, Font color: Auto

Formatted: Hyperlink, No underline, Underline color: Auto, Font color: Auto

Formatted: Indent: Left: 0.85 cm, Hanging: 0.85 cm, Right: 0 cm, Space Before: 12 pt, After: 12 pt, Line spacing: 1.5 lines

Formatted: Indent: Left: 0.85 cm, Hanging: 0.85 cm, Right: 0 cm, Space Before: 12 pt, After: 12 pt, Line spacing: 1.5 lines

Formatted: Indent: Left: 0.85 cm, Hanging: 0.85 cm, Right: 0 cm, Space Before: 12 pt, After: 12 pt, Line spacing: 1.5 lines

Formatted: Header

Litzow, M. A., Malick, M. J., Bond, N. A., Cunningham, C. J., Gosselin, J. L., & Ward, E. J. (2020). Quantifying a Novel Climate Through Changes in PDO-Climate and ~~PDO~~~~Salmon~~~~PDO-Salmon~~ Relationships. *Geophysical Research Letters*, 47(16), e2020GL087972. <https://doi.org/10.1029/2020GL087972>

Liu, Y., Sun, C., Kucharski, F., Li, J., Wang, C., & Ding, R. (2021). The North Pacific Blob acts to increase the predictability of the Atlantic warm pool. *Environmental Research Letters*, 16(6), 064034. <https://doi.org/10.1088/1748-9326/ac0030>

Lysne, J. A., Chang, P., & Giese, B. (1997). Impact of the extratropical Pacific on equatorial variability. *Geophysical Research Letters*, 24(21), 2589–2592. <https://doi.org/10.1029/97GL02751> <https://doi.org/10.1029/97GL02751>

~~Mantua, N. J., Hare, S. R., Zhang, Y., Wallace, J. M., & Francis, R. C. (1997). A Pacific Interdecadal Climate Oscillation with Impacts on Salmon Production. *Bulletin of the American Meteorological Society*, 78(6), 1069–1079. [https://doi.org/10.1175/1520-0477\(1997\)078<1069:APICOW>2.0.CO;2](https://doi.org/10.1175/1520-0477(1997)078<1069:APICOW>2.0.CO;2)~~

Mahajan, S., Saravanan, R., & Chang, P. (2009). The role of the wind-evaporation-sea surface temperature (WES) feedback in air-sea coupled tropical variability. *Atmospheric Research*, 94(1), 19–36. <https://doi.org/10.1016/j.atmosres.2008.09.017>

~~*Atmospheric Research*, 94(1), 19–36. <https://doi.org/10.1016/j.atmosres.2008.09.017>~~

Martin, Z., Orbe, C., Wang, S., & Sobel, A. (2021). The MJO–QBO relationship in a GCM with stratospheric nudging. *Journal of Climate*, 34(11), 4603–4624. <https://doi.org/10.1175/JCLI-D-20-0636.1>

McCreary, J. P., & Peng Lu. (1994). Interaction between the subtropical and equatorial ocean circulations: the subtropical cell. *Journal of Physical Oceanography*, 24(2), 466–497. [https://doi.org/10.1175/1520-0485\(1994\)024<0466:IBTSAE>2.0.CO;2](https://doi.org/10.1175/1520-0485(1994)024<0466:IBTSAE>2.0.CO;2)

~~466–497. [https://doi.org/10.1175/1520-0485\(1994\)024<0466:IBTSAE>2.0.CO;2](https://doi.org/10.1175/1520-0485(1994)024<0466:IBTSAE>2.0.CO;2)~~

Nagano, A., & Wakita, M. (2019). Wind-driven decadal sea surface height and main pycnocline depth changes in the western subarctic North Pacific. *Progress in Earth and Planetary Science*, 6(1), 1–26. <https://doi.org/10.1186/s40645-019-0303-0>

Formatted: Indent: Left: 0.85 cm, Right: 0 cm, Space Before: 12 pt, After: 12 pt, Line spacing: 1.5 lines

Formatted: Indent: Left: 0.85 cm, Right: 0 cm, Space Before: 12 pt, After: 12 pt, Line spacing: 1.5 lines

585 Newman, M., Alexander, M. A., Ault, T. R., Cobb, K. M., Deser, C., Di Lorenzo, E., Mantua,  
586 N. J., Miller, A. J., Minobe, S., Nakamura, H., Schneider, N., Vimont, D. J., Phillips, A.  
587 S., Scott, J. D., & Smith, C. A. (2016). The Pacific decadal oscillation, revisited. *Journal*  
588 *of Climate*, 29(12), 4399–4427. <https://doi.org/10.1175/JCLI-D-15-0508.1>

589 ~~S., Scott, J. D., & Smith, C. A. (2016). The Pacific decadal oscillation, revisited.~~  
590 ~~*Journal of Climate*, 29(12), 4399–4427. <https://doi.org/10.1175/JCLI-D-15-0508.1>~~

591 Pickart, R. S., Moore, G. W. K., Macdonald, A. M., Renfrew, I. A., Walsh, J. E., & Kessler,  
592 W. S. (2009). Seasonal evolution of Aleutian low pressure systems: Implications for the  
593 North Pacific subpolar circulation. *Journal of Physical Oceanography*, 39(6), ~~1317–~~  
594 ~~1339. <https://doi.org/10.1175/2008JPO3891.1>~~

595 ~~1317–1339. <https://doi.org/10.1175/2008JPO3891.1>~~

596 Pierce, D. W., Barnett, T. P., & Latif, M. (2000). Connections between the Pacific Ocean  
597 Tropics and midlatitudes on decadal timescales. *Journal of Climate*, 13(6), 1173–  
598 1194. [https://doi.org/10.1175/1520-0442\(2000\)013<1173:CBTPOT>2.0.CO;2](https://doi.org/10.1175/1520-0442(2000)013<1173:CBTPOT>2.0.CO;2)

599 Richter, J. H., Deser, C., & Sun, L. (2015). Effects of stratospheric variability on El Niño.  
600 *Environmental Research Letters*, 10(12). [https://doi.org/10.1088/174893261748-](https://doi.org/10.1088/174893261748-9326/10/12/124021)  
601 ~~9326/10/12/124021~~

602 Schneider, N., & Cornuelle, B. D. (2005). The forcing of the Pacific Decadal Oscillation.  
603 *Journal of Climate*, 18(21), 4355–4373. <https://doi.org/10.1175/JCLI3527.1>

604 Schneider, N., Miller, A. J., & Pierce, D. W. (2002). Anatomy of North Pacific decadal  
605 variability. In *Journal of Climate* (Vol. 15, Issue 6). [https://doi.org/10.1175/1520-](https://doi.org/10.1175/1520-0442(2002)015<0586:AONPDV>2.0.CO;2)  
606 ~~0442(2002)015<0586:AONPDV>2.0.CO;2~~

607 ~~0442(2002)015<0586:AONPDV>2.0.CO;2~~

608 Simon, A., Gastineau, G., Frankignoul, C., Rousset, C., & Codron, F. (2021). Transient  
609 climate response to Arctic Sea ice loss with two ice-constraining methods. *Journal of*  
610 *Climate*, 34(9), 3295–3310. <https://doi.org/10.1175/JCLI-D-20-0288.1>

Formatted: Header

Formatted: Indent: Left: 0.85 cm, Hanging: 0.85 cm, Right: 0 cm, Space Before: 12 pt, After: 12 pt, Line spacing: 1.5 lines

Formatted: Indent: Left: 0.85 cm, Hanging: 0.85 cm, Right: 0 cm, Space Before: 12 pt, After: 12 pt, Line spacing: 1.5 lines

Formatted: Indent: Left: 0.85 cm, Hanging: 0.85 cm, Right: 0 cm, Space Before: 12 pt, After: 12 pt, Line spacing: 1.5 lines

Formatted: Indent: Left: 0.85 cm, Hanging: 0.85 cm, Right: 0 cm, Space Before: 12 pt, After: 12 pt, Line spacing: 1.5 lines

Formatted: Indent: Left: 0.85 cm, Right: 0 cm, Space Before: 12 pt, After: 12 pt, Line spacing: 1.5 lines

- 611 Smith, D. M., Booth, B. B. B., Dunstone, N. J., Eade, R., Hermanson, L., Jones, G. S.,  
612 Scaife, A. A., Sheen, K. L., & Thompson, V. (2016). Role of volcanic and  
613 anthropogenic aerosols in the recent global surface warming slowdown. *Nature*  
614 *Climate Change*, 6(10), 936–940. <https://doi.org/10.1038/nclimate3058>
- 615 Sugimoto, S., & Hanawa, K. (2009). Decadal and interdecadal variations of the Aleutian  
616 Low activity and their relation to upper oceanic variations over the North Pacific.  
617 *Journal of the Meteorological Society of Japan*, 87(4), 601–614.  
618 <https://doi.org/10.2151/jmsj.87.601>
- 619 ~~*Journal of the Meteorological Society of Japan*, 87(4), 601–614.~~  
620 ~~<https://doi.org/10.2151/jmsj.87.601>~~
- 621 Sun, J., & Wang, H. (2006). Relationship between Arctic Oscillation and Pacific Decadal  
622 Oscillation on decadal timescale. *Chinese Science Bulletin*, 51(1), 75–79.  
623 <https://doi.org/10.1007/s11434-004-0221-3>
- 624 Sun, T., & Okumura, Y. M. (2019). Role of stochastic atmospheric forcing from the south  
625 and North Pacific in tropical Pacific decadal variability. *Journal of Climate*, 32(13),  
626 ~~4013–4038. <https://doi.org/10.1175/JCLI-D-18-0536.1>~~  
627 ~~4013–4038. <https://doi.org/10.1175/JCLI-D-18-0536.1>~~
- 628 Taguchi, B., Xie, S. P., Schneider, N., Nonaka, M., Sasaki, H., & Sasai, Y. (2007). Decadal  
629 variability of the Kuroshio Extension: Observations and an eddy-resolving model  
630 hindcast. *Journal of Climate*, 20(11), 2357–2377. <https://doi.org/10.1175/JCLI4142.1>
- 631 Trenberth, K. E., & Hurrell, J. W. (1994). Decadal atmosphere-ocean variations in the  
632 Pacific. *Climate Dynamics*, 9(6), 303–319. <https://doi.org/10.1007/BF00204745>
- 633 Vimont, D. J. (2005). The contribution of the interannual ENSO cycle to the spatial pattern  
634 of decadal ENSO-like variability. In *Journal of Climate* (Vol. 18, Issue 12).  
635 <https://doi.org/10.1175/JCLI3365.1>
- 636 Vimont, D. J., Battisti, D. S., & Hirst, A. C. (2001). Footprinting: A seasonal connection  
637 between the tropics and mid-latitudes. *Geophysical Research Letters*, 28(20), 3923–  
638 ~~3926. <https://doi.org/10.1029/2001GL013435>~~

Formatted: Header

Formatted: Indent: Left: 0.85 cm, Hanging: 0.85 cm, Right: 0 cm, Space Before: 12 pt, After: 12 pt, Line spacing: 1.5 lines

Formatted: Indent: Left: 0.85 cm, Hanging: 0.85 cm, Right: 0 cm, Space Before: 12 pt, After: 12 pt, Line spacing: 1.5 lines

Formatted: Indent: Left: 0.85 cm, Hanging: 0.85 cm, Right: 0 cm, Space Before: 12 pt, After: 12 pt, Line spacing: 1.5 lines

639 ~~3926-<https://doi.org/10.1029/2001GL013435>~~

640 Vimont, D. J., Battisti, D. S., & Hirst, A. C. (2002). Pacific interannual and interdecadal  
641 equatorial variability in a 1000-Yr simulation of the CSIRO coupled general circulation  
642 model. *Journal of Climate*, 15(2), 160–178. [https://doi.org/10.1175/1520-](https://doi.org/10.1175/1520-0442(2002)015<0160:PIAIEV>2.0.CO;2)  
643 [0442\(2002\)015<0160:PIAIEV>2.0.CO;2](https://doi.org/10.1175/1520-0442(2002)015<0160:PIAIEV>2.0.CO;2)

644 ~~0442(2002)015<0160:PIAIEV>2.0.CO;2~~

645 Vimont, D. J., Wallace, J. M., & Battisti, D. S. (2003). The seasonal footprinting mechanism  
646 in the Pacific: Implications for ENSO. *Journal of Climate*, 16(16), 2668–2675.  
647 [https://doi.org/10.1175/1520-0442\(2003\)016<2668:TFSMIT>2.0.CO;2](https://doi.org/10.1175/1520-0442(2003)016<2668:TFSMIT>2.0.CO;2)

648 Wang, H., Kumar, A., Wang, W., & Xue, Y. (2012). Seasonality of the Pacific decadal  
649 oscillation. *Journal of Climate*, 25(1), 25–38. <https://doi.org/10.1175/2011JCLI4092.1>

650 Watson, P. A. G., Weisheimer, A., Knight, J. R., & Palmer, T. N. (2016). The role of the  
651 tropical West Pacific in the extreme Northern Hemisphere winter of 2013/2014. *Journal*  
652 *of Geophysical Research*, 121(4), 1698–1714. <https://doi.org/10.1002/2015JD024048>

653 ~~*Journal of Geophysical Research*, 121(4), 1698–1714.~~  
654 ~~<https://doi.org/10.1002/2015JD024048>~~

655 Webb, D. J. (1996). An ocean model code for array processor computers. *Computers and*  
656 *Geosciences*, 22(5), 569–578. [https://doi.org/10.1016/0098-3004\(95\)00133-6](https://doi.org/10.1016/0098-3004(95)00133-6)

657 Wills, R. C. J., Battisti, D. S., Proistosescu, C., Thompson, L. A., Hartmann, D. L., &  
658 Armour, K. C. (2019). Ocean Circulation Signatures of North Pacific Decadal  
659 Variability. *Geophysical Research Letters*, 46(3), 1690–1701.  
660 <https://doi.org/10.1029/2018GL080716>

661 Xie, S. P., & Tanimoto, Y. (1998). A pan-Atlantic decadal climate oscillation. *Geophysical*  
662 *Research Letters*, 25(12), 2185–2188. <https://doi.org/10.1029/98GL01525>

663 Zhang, D., & McPhaden, M. J. (2006). Decadal variability of the shallow Pacific meridional  
664 overturning circulation: Relation to tropical sea surface temperatures in observations  
665 and climate change models. *Ocean Modelling*, 15(3–4), 250–273.  
666 <https://doi.org/10.1016/j.ocemod.2005.12.005>

Formatted: Header

Formatted: Indent: Left: 0.85 cm, Hanging: 0.85 cm, Right: 0 cm, Space Before: 12 pt, After: 12 pt, Line spacing: 1.5 lines

Formatted: Indent: Left: 0.85 cm, Hanging: 0.85 cm, Right: 0 cm, Space Before: 12 pt, After: 12 pt, Line spacing: 1.5 lines

Formatted: Indent: Left: 0.85 cm, Hanging: 0.85 cm, Right: 0 cm, Space Before: 12 pt, After: 12 pt, Line spacing: 1.5 lines

Formatted: Indent: Left: 0.85 cm, Hanging: 0.85 cm, Right: 0 cm, Space Before: 12 pt, After: 12 pt, Line spacing: 1.5 lines

667 Zhang, Y., Xie, S. P., Kosaka, Y., & Yang, J. C. (2018). Pacific decadal oscillation: Tropical  
668 Pacific forcing versus internal variability. *Journal of Climate*, 31(20), 8265–8279.  
669 <https://doi.org/10.1175/JCLI-D-18-0164.1>  
670 ~~<https://doi.org/10.1175/JCLI-D-18-0164.1>~~  
671 Zhao, Y., Newman, M., Capotondi, A., Lorenzo, E. Di, & Sun, D. (2021). Removing the  
672 effects of tropical dynamics from north pacific climate variability. *Journal of Climate*,  
673 34(23), 9249–9265. <https://doi.org/10.1175/JCLI-D-21-0344.1>

Formatted: Header

Formatted: Indent: Left: 0.85 cm, Hanging: 0.85 cm,  
Right: 0 cm, Space Before: 12 pt, After: 12 pt, Line  
spacing: 1.5 lines

674  
675  
676  
677  
678  
679  
680  
681  
682  
683  
684  
685  
686  
687  
688  
689  
690  
691  
692  
693  
694  
695  
696  
697  
698

**Figures**

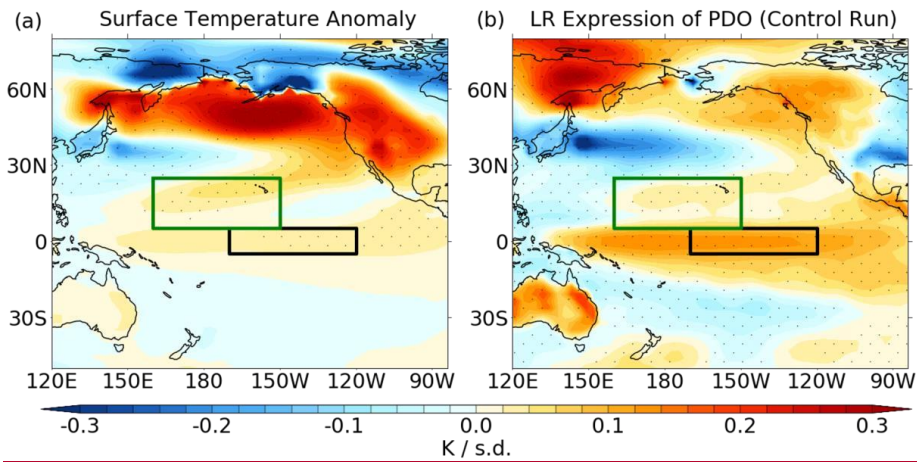
Formatted: Underline color: Auto

Formatted: Space After: 0 pt, Line spacing: 1.5 lines

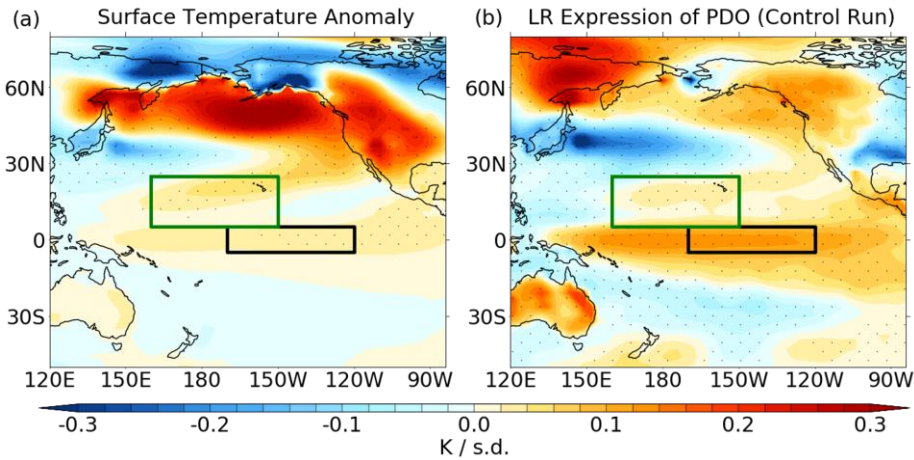
Formatted: Font: 12 pt, Bold, Underline, Font color:  
Black, , Ligatures: Standard + Contextual



699  
700  
701



702  
703  
704  
705

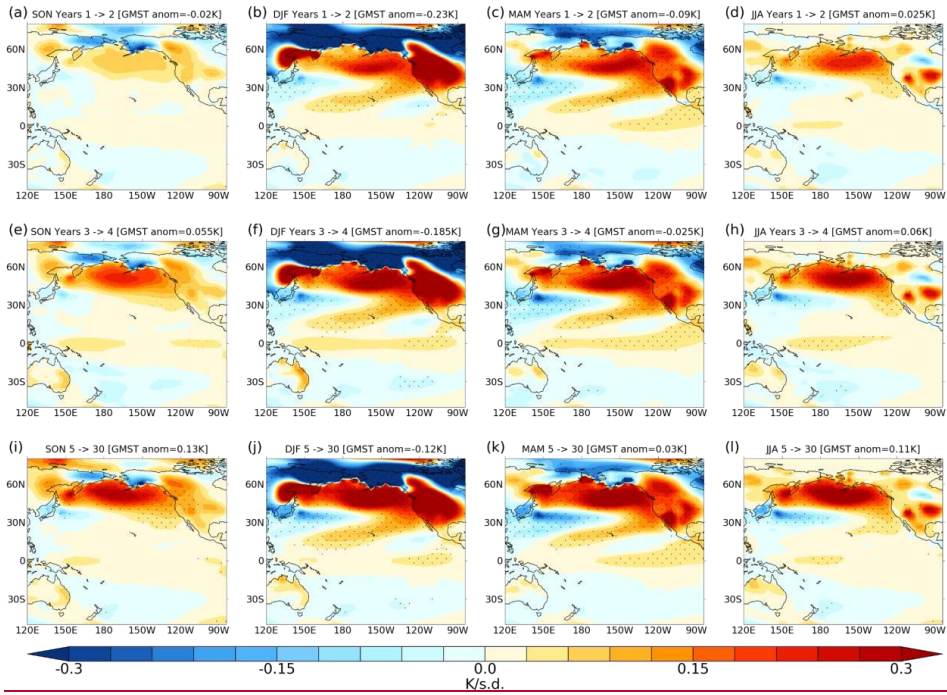


706

707 **Figure 1:** Annual mean surface temperature anomalies for (a) ~~regression onto the PDO~~  
708 ~~index in CONTROL~~; (b) ensemble mean anomaly in NUDGED averaged over years 1-30;  
709 ~~(b) regression onto the PDO index in CONTROL~~. Units are K per standard deviation.

710 Stippling denotes anomalies that are significant at the 95% level. Green and black boxes  
711 show the regions for the mixed layer heat budget analysis.

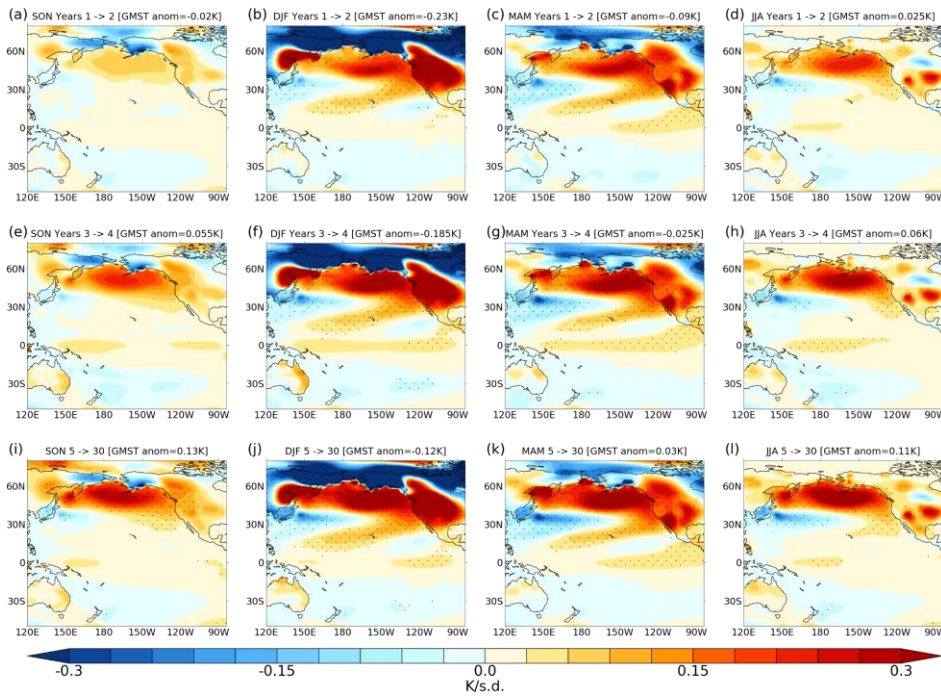
712



713

714

Formatted: Header



715

716

717 **Figure 2:** Seasonal mean surface temperature anomalies in NUDGED expressed per unit  
718 PDO index [K/σ] for SON, DJF, MAM and JJA. AnomaliesComposite anomalies are shown  
719 for years 1-2 (a-d), years 3-4 (e-h) and years 5-30 (i-l). Global mean surface temperature  
720 anomalies are shown in the header. Stippling denotes anomalies that are significant at the  
721 95% level.

722

723

724

725

726

727

728

729

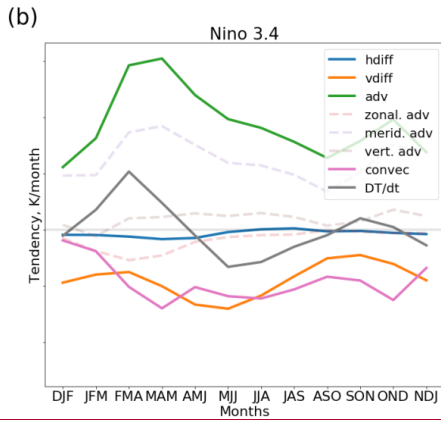
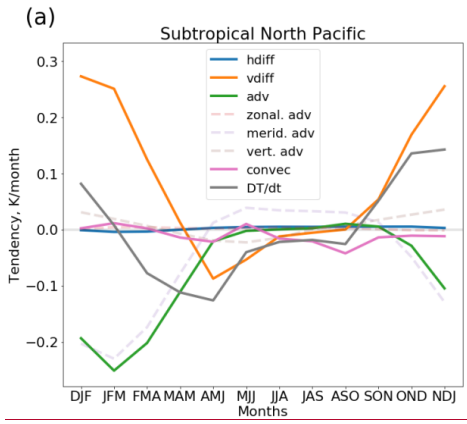
730

Formatted: Space After: 0 pt, Line spacing: 1.5 lines

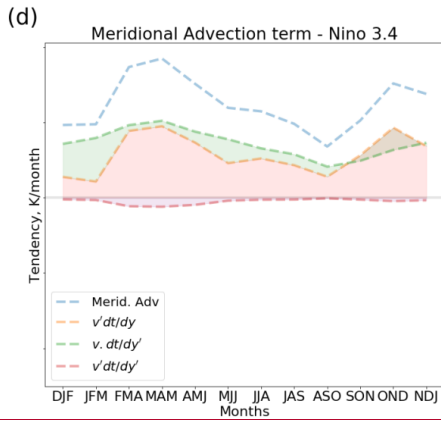
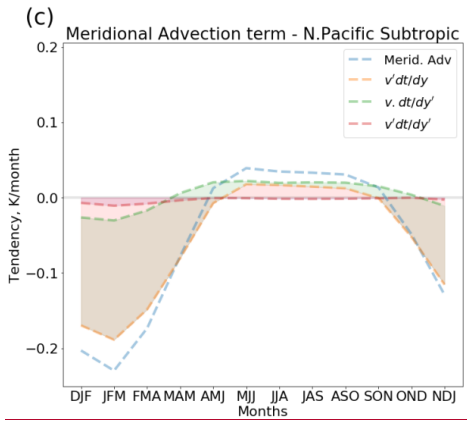
Formatted: Justified, Indent: Left: 0 cm, Right: 0 cm,  
Space After: 6 pt, Line spacing: 1.5 lines

Formatted: Font: Symbol, 11 pt, Not Superscript/  
Subscript

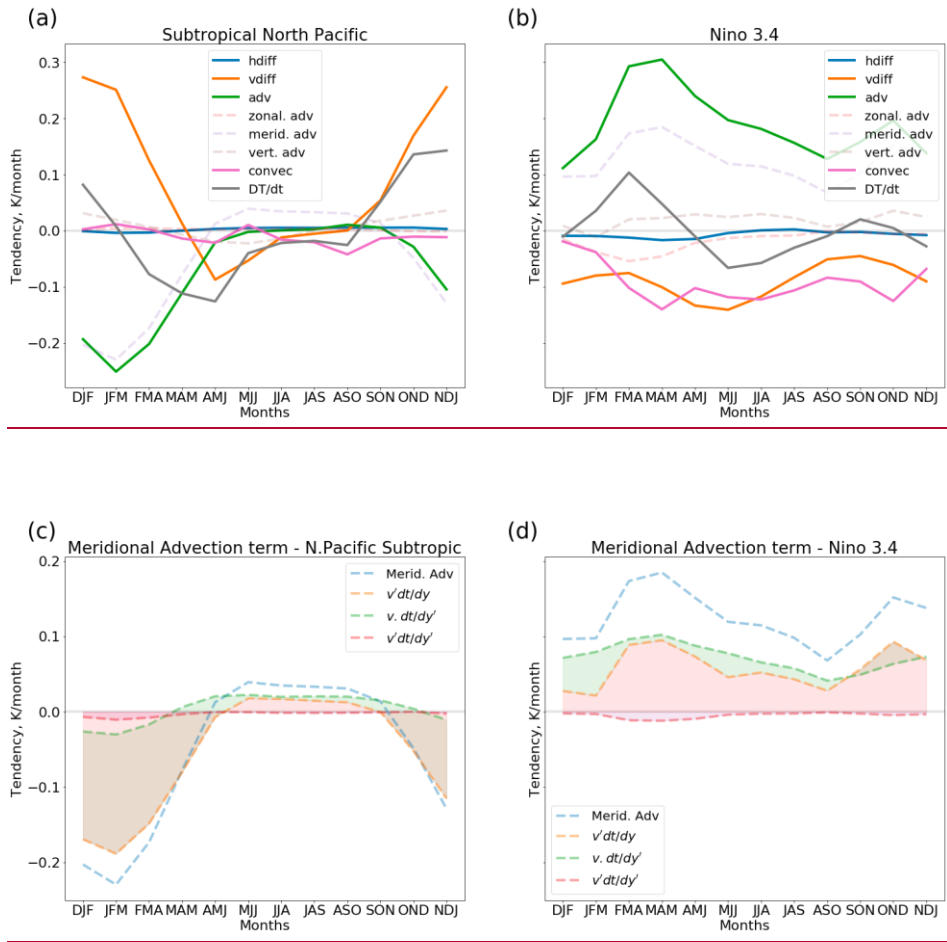
731  
732



733  
734  
735



736  
737  
738  
739  
740  
741  
742  
743  
744

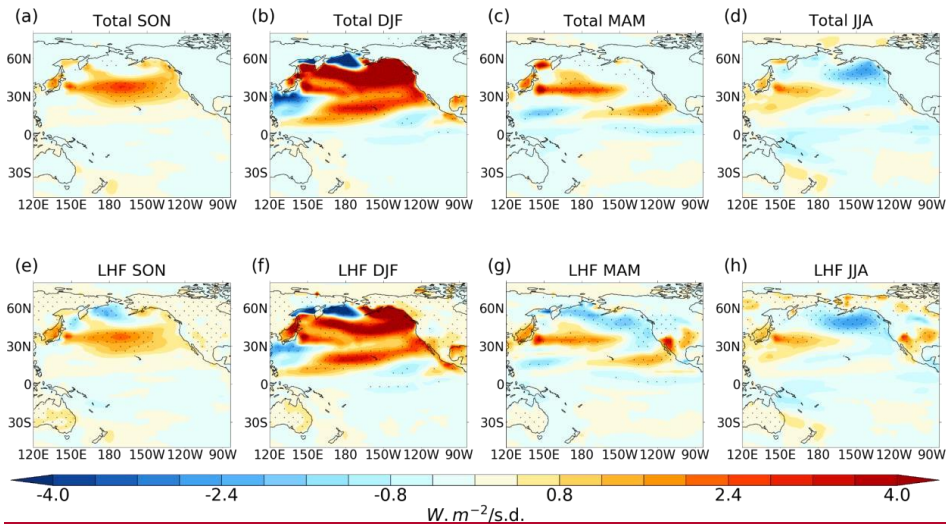


745  
746  
747  
748  
749  
750  
751  
752 **Figure 3:** Years 1-30, 3-month moving average of anomalous NUGGED-CONTROL  
753 mixed layer temperature tendencies and constituent heat budget terms for the (a)  
754 subtropical North Pacific and (b) Niño 3.4 regions. (c,d) show the meridional advection  
755 term and its linear expansion.

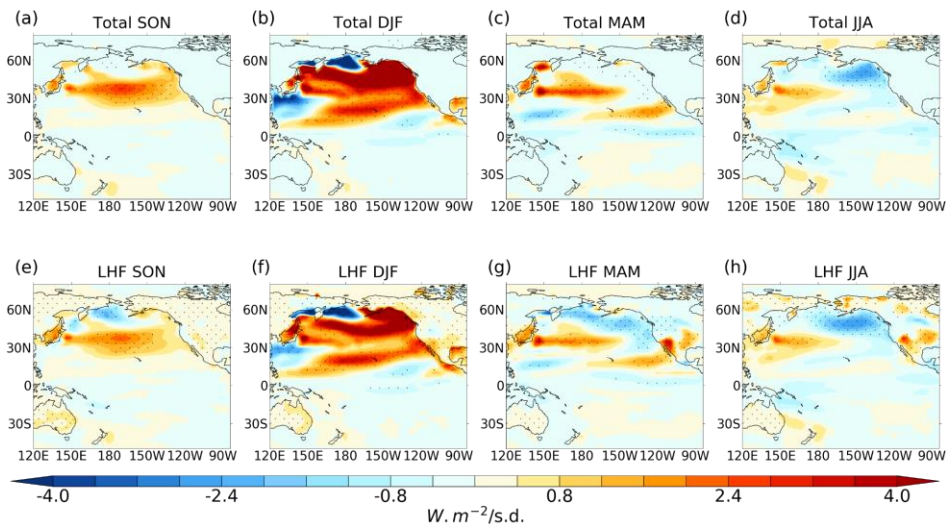
Formatted: Justified, Indent: Left: 0 cm, Right: 0 cm, Space After: 6 pt, Line spacing: 1.5 lines

Formatted: Font: 12 pt





756



757

758 **Figure 4:** (a-d) Seasonal Years 1-30 seasonal mean net surface heat flux anomalies in  
759 NUDGED. (e-h):

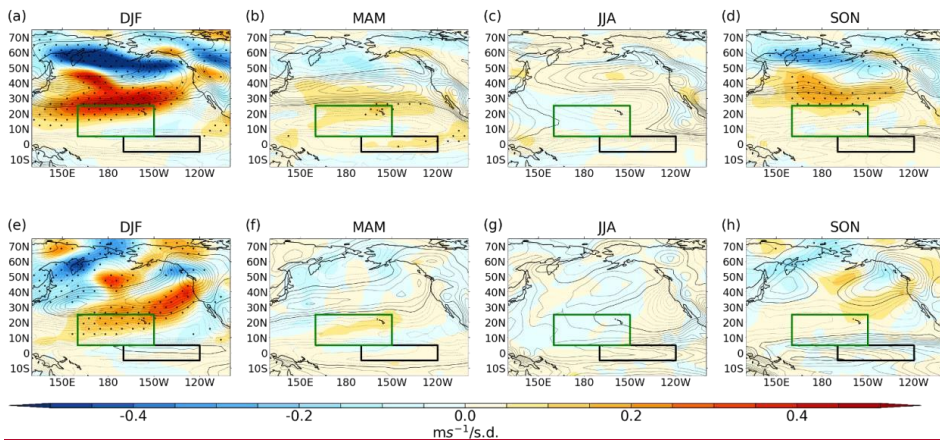
760 Seasonal Years 1-30 seasonal mean latent heat flux anomaly in NUDGED. Positive  
761 denotes downward flux.

762 Stippling denotes anomalies that are statistically significant at the 95% level. Units:  $W \cdot m^{-2}$   
763  $m^{-2}$  per standard deviation.

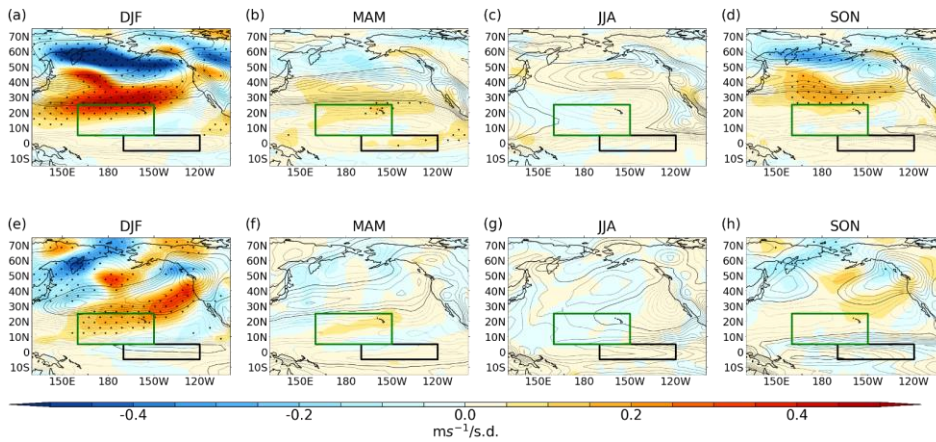
Formatted: Justified, Indent: Left: 0 cm, Right: 0 cm,  
Space After: 6 pt, Line spacing: 1.5 lines

Formatted: Font: 12 pt

764  
765  
766  
767  
768  
769  
770  
771  
772  
773  
774  
775  
776  
777



Formatted: Header



778

779

780 **Figure 5:** Seasonal mean NUDGED-CONTROL near-surface wind  
781 anomalies for (a-d) zonal and (e-  
782 h) meridional wind. Contours show climatology of CONTROL (dashed lines are negative  
783 values, contour interval  $1 \text{ m s}^{-1}$ ). Stippling denotes anomalies that are significant at the  
784 95% level.

Formatted: Justified, Indent: Left: 0 cm, Right: 0 cm,  
Space After: 6 pt, Line spacing: 1.5 lines

Formatted: Font: 12 pt

785

786

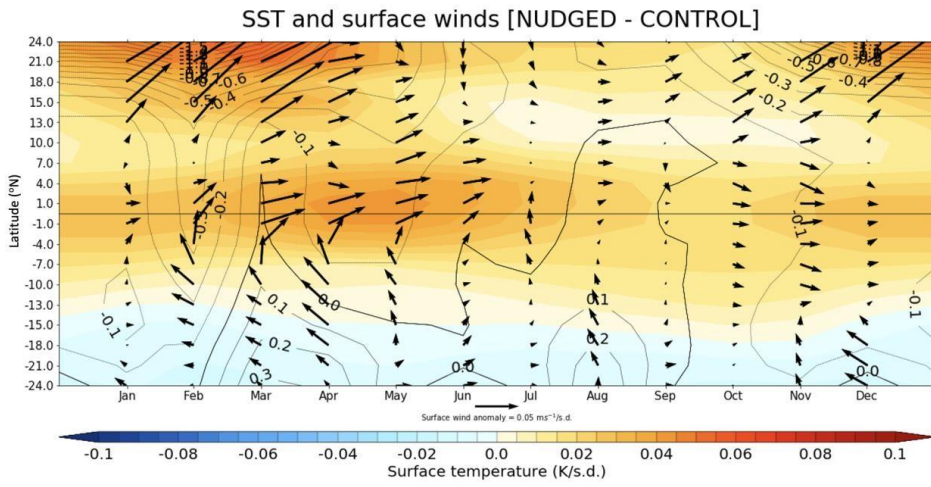
787

788

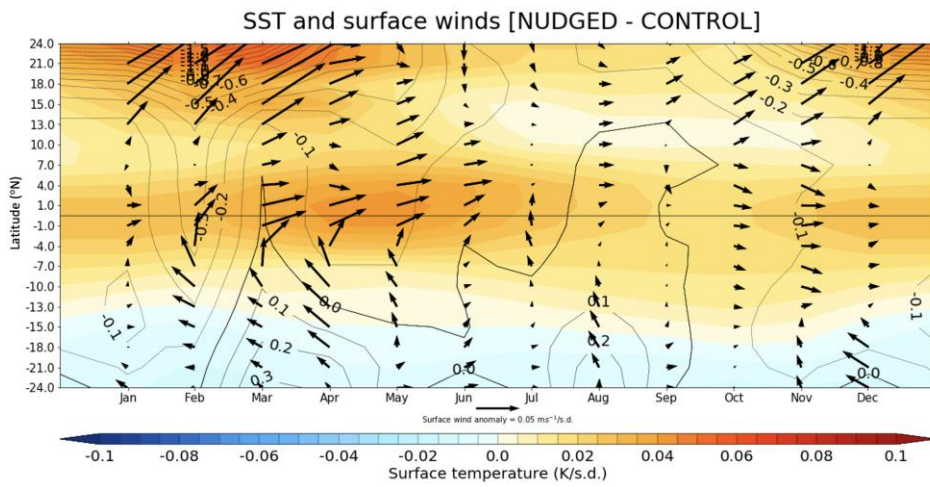
789

790





791  
792  
793  
794  
795  
796  
797  
798



799

800

801 **Figure 6:** Latitude-time section of **NUDGED-CONTROL** SST anomaly  
802 (K/s.d.: shading), surface pressure (hPa/s.d.: contours) and near-surface wind anomaly (m s<sup>-1</sup>/s.d.: vectors) averaged over the **central-eastern** tropical Pacific (205°W-  
803 80°W).

Formatted: Justified, Indent: Left: 0 cm, Right: 0 cm, Space After: 6 pt, Line spacing: 1.5 lines

Formatted: Font: Symbol, 11 pt, Not Superscript/Subscript

Formatted: Font: Symbol, 11 pt, Not Superscript/Subscript

Formatted: Font: Symbol, 11 pt, Not Superscript/Subscript

Formatted: Font: 12 pt

805

806

807

808

809

810

811

812

813

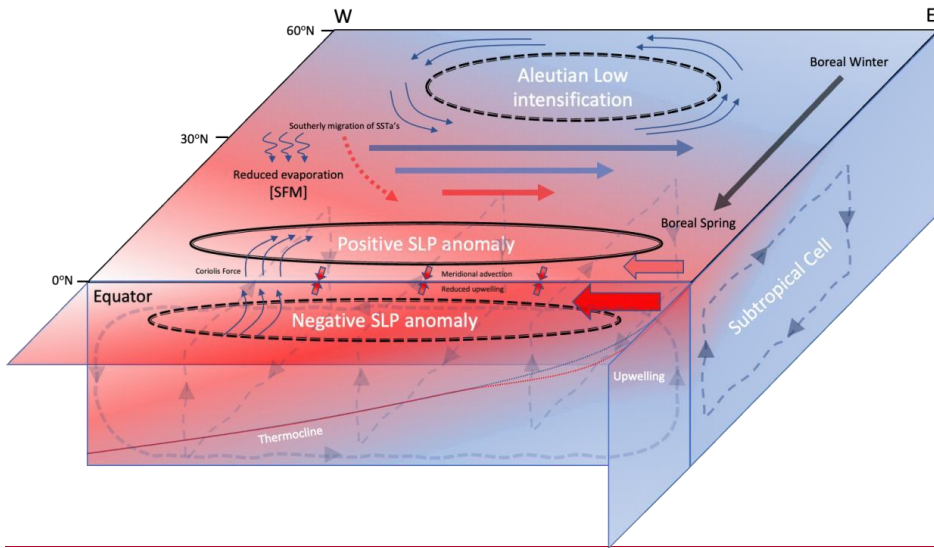
814

815

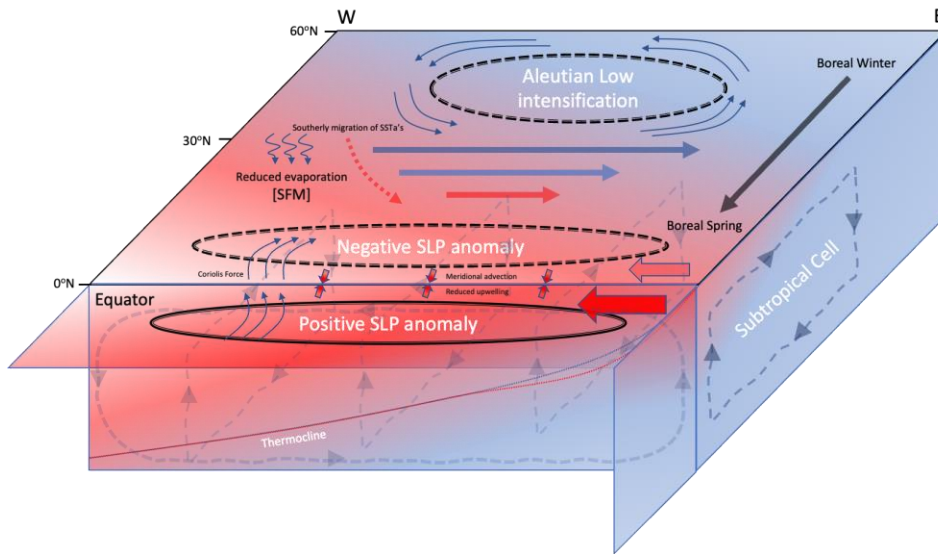
816

817

818



819  
820  
821  
822  
823  
824  
825  
826  
827  
828  
829  
830  
831  
832  
833  
834  
835



836

837 **Figure 7:** Schematic depicting the mechanisms involved in the tropical SST anomalies  
838 manifest as a result from an intensification of the AL. An intensified AL (dashed black  
839 line) imposed during boreal winter is associated with intensified westerlies (solid arrows)  
840 in the extra-tropics and downward latent heat transfer. The migration of the SST  
841 anomalies southward during boreal winter is associated with a southerly shift in the  
842 westerly anomalies. The westerly anomalies act to weaken the background trades (filled  
843 red arrows) which reduce latent heating due to evaporation and hence an increase in  
844 extra-tropical Pacific SSTs. In the season after nudging, the temperature asymmetry  
845 either side of the equator induces an SLP gradient (solid line – positive SLP; dashed line  
846 – negative SLP) that drives southerly winds across the equator. The Coriolis force acts  
847 to turn the southerly winds in the southern hemisphere westward and in the northern  
848 hemisphere eastward. When these anomalous winds are imposed on the background  
849 easterly trade winds (filled red arrows), the southerlies south of the equator increase the  
850 wind speed and therefore evaporative cooling, whilst north of the equator the  
851 background trades are weakened, reducing evaporative cooling. The changes to the  
852 wind driven surface state act to deepen the thermocline in the eastern tropical Pacific  
853 (red dotted line) and reduce upwelling/divergence of cooler waters at the equator.

|

854 \_\_\_\_\_

855 \_\_\_\_\_

856 \_\_\_\_\_

857 647 \_\_\_\_\_

858 \_\_\_\_\_

859 \_\_\_\_\_

860

Formatted: Header

Formatted: Footer distance from edge: 1.27 cm,  
Numbering: Continuous

Formatted: Indent: Left: 0 cm, Line spacing: 1.5 lines,  
Tab stops: Not at 0 cm

|

1 \_\_\_\_\_ 1

Formatted: Line spacing: single, Tab stops: Not at 8.26  
cm